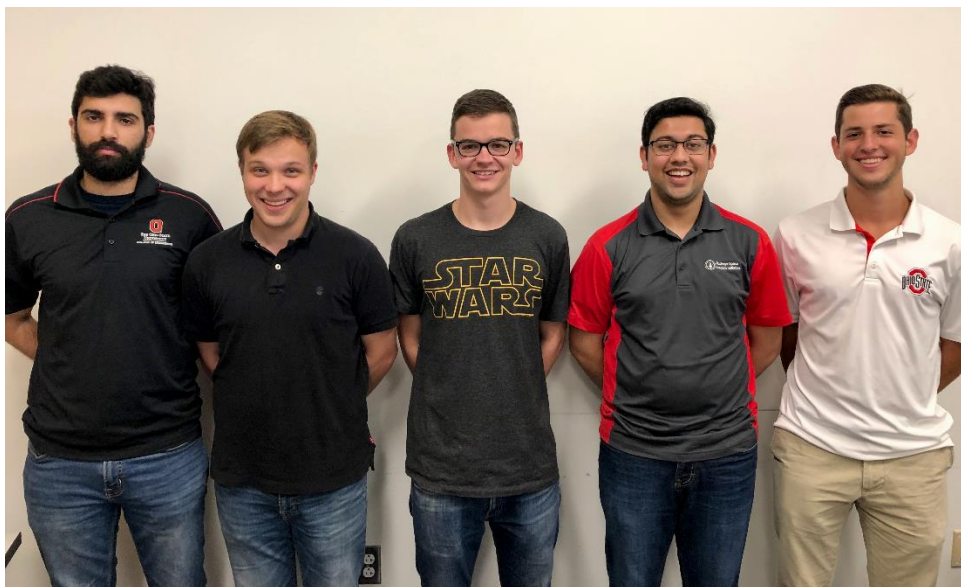


Designing a Process Model for the JetCat P180x

The Ohio State University



Team Members (Left to Right):

Isaac Khan	Engineering Physics
Ross Heidersbach	Mechanical Engineering
Tommy Malkus	Engineering Physics
Hamil Shah	Electrical Engineering
Mark Luke	Mechanical Engineering

Dr. Matthew McCrink
Department of Mechanical and Aerospace Engineering
The Ohio State University

ENGR 5901.01 Autumn 2018

December 7th, 2018

Change of Notice

Revision #	Reviser	Reason for Change	Date
1	Team	Document Created	10/4/2019
2	Team	Revised Problem Definition	11/4/2018
3	Team	Added Systems Design Section	11/6/2018
4	Team	Revised and Added Detailed Design	12/7/2018

Design Changes

Following feedback from the Preliminary Design Review, the following items have been updated:

1. Adapted the test stand to be mounted to the 3'x5' wind tunnel
2. Split the large airfoil into sections that connect to the front and back of the vertical bar
3. Added a vertical support beam at the end of the test stand nearest to the load cell
4. Conducted further analysis on horizontal beam and bolting failure (see Systems Design Section)

Table of Contents

Change of Notice.....	2
Design Changes	3
Table of Contents.....	4
List of Figures	6
List of Tables	7
Chapter 1 - Problem Definition.....	8
Interpretation of Project	8
Primary Research	8
Final Problem Definition	8
Secondary Research	10
Needs Chart.....	11
Chapter 2 – Systems Design.....	13
Development of Concepts.....	13
Description of Selected Concept and Rationale.....	16
Identify Metrics and Requirements	17
Detail Design	32
Development of Detail Design	32
Assembly and Manufacturing Procedures	36
Prototype Plan.....	36
Prototype Risk Assessment	38
Budget Breakdown.....	52
Sponsor Feedback	Error! Bookmark not defined.
Current Progress and Future Considerations.....	Error! Bookmark not defined.
References	55
Appendix	56
Original Problem Statement	56
Team Charter.....	57
Problem Definition Presentation	64
Preliminary Design Review.....	67
Critical Design Review Presentation	71
Project Schedule.....	75

Team Meeting Notes..... 76

List of Figures

Figure 1.1: JetCat thrust stand.....	9
Figure 1.2: Moment Arm Thrust Stand	9
Figure 2.1: Thrust Stand Structural Concepts	13
Figure 2.2: Adapter Design Concepts.....	14
Figure 2.3 Airfoil Design	15
Figure 2.4 Overall Design of Thrust Stand	17
Figure 2.5: Free Body Diagram of Vertical Beam.....	20
Figure 2.6: Shear-Moment Diagram of Vertical Beam	21
Figure 2.7: Visualization of the Loading Modes Located at Beam's Base	22
Figure 2.8: Visualization of Cantilever Beam Bending	23
Figure 2.9: Free Body Diagram of Horizontal Beam	26
Figure 2.10: Shear-Moment Diagram of Horizontal Beam	27
Figure 2.11: Bolting groups selected for failure analysis.....	30
Figure 2.12: Bolting stress values and safety factors for range of thrusts.	31
Figure 3.1 3D View of Final Thrust Stand Design.....	33
Figure 3.2 Front View of Final Thrust Stand Design.....	34
Figure 3.3 Profile and Dimensions of Final Thrust Stand Design.....	34
Figure 3.4 Bill of Materials	36
Figure 3.5 Experiment Testing Matrix.....	37
Figure 3.6 Test Process and Validation Plan	37
Figure A.1: Gantt Chart	75
Figure A.2 Exploded View of Preliminary Design.....	79
Figure A.3 Breakdown of the Additional Materials from the Detail Design B.O.M.....	80
Figure A.4: Bolting group calculations for the four different groups.	85
Figure A.5: Bolting group stress figures using max shear stress failure theory.	87
Figure A.6: Bolting group safety factors using max shear stress failure theory.	89

List of Tables

Table 1.1: Outline of Design Needs	12
Table 1.2: Designs Scored	12
Table 2.1 Structural Design Screening	14
Table 2.2 Adapter Designs Scored	15
Table 2.3: Airfoil Designs Considered	16
Table 2.4: Airfoil Screening Matrix	16
Table 2.5: Measurable Metrics for each Need	17
Table 2.6: Measurable Metrics for each Need	18
Table 2.7. Desired Metric Value and Acceptable Ranges	19
Table 2.8: Mechanical and Loading Properties of Vertical Beam Designs	25
Table 2.9: Mechanical and Loading Properties of Horizontal Beam Designs	29
Table 3.1: Failure Modes.....	35
Table 3.2 Budget Breakdown.....	52

Chapter 1 - Problem Definition

Interpretation of Project

Over the past four years, Dr. McCrink and other research scientists at The Ohio State University's Aerospace Research Center have been focusing efforts on advancing the forefront of Unmanned Aerial Vehicle (UAV) technology. Specifically, Dr. McCrink has been researching turbine powered UAVs and self-tuning autopilots in order to progress UAV control technology and break world records for both average flight speed and maximum range. During previous flight tests, collected engine data suggested that the UAV's engine controller was operating at its performance envelope and could marginally manipulate the jet turbine in a stable manner during demanding and dynamic phases of flight. The controller's inability to manipulate the engine in a stable and predictable manner is a result of not having an accurate mathematical model of the turbine engine during its transient response to varying inputs and environmental conditions. The overarching objective of this capstone is to produce a plant model of the JetCat P180 turbine engine that allows for the accurate prediction of its transient response; such data would allow more effective autopilots to be built for future projects.

Based off of the brief problem statement described above, it was initially assumed that research would be conducted only on the transient nature of the JetCat P180 turbine engine. From this guiding assumption, an initial hypothesis was formulated that a mathematical model, known as a plant model, could be imperially formulated to predict the response of the turbine by collecting experimental data. By subjecting the engine to a variety of initial conditions and commanded inputs, the resulting response could be measured and general relationships between engine inputs and outputs could be realized. This type of plant model derivation is known as System Identification, and heavily relies on both experimental data and differential equation curve fitting techniques to experimentally compute a transfer function for the system or device under investigation. Once a general plant model of the JetCat P180 is derived, the transfer function can be implemented into a variety of UAV projects which utilize feedback control laws to manipulate the micro-turbojet.

Primary Research

An initial meeting with Dr. McCrink was held to introduce the team and to develop an understanding about what the JetCat project would entail; meeting notes can be found in the appendix. With Dr. McCrink being the only primary stakeholder in the project, information about the JetCat P180x and research to be done was derived from the first two meetings. Research was done to gain a better understanding of the engine itself and how it could be modelled. The literature review explored many papers on the steady state modeling of small turbojet engines through analytical means [1-5], and few on the transient response of the engines [1, 8]. Based off of the information gathered via the review, it was decided to derive an analytical model for the engine which would be tested experimentally later in the year.

Final Problem Definition

Dr. McCrink's fundamental need is to improve the active control of jet powered UAVs, which currently cannot be done well as there is not an accurate dynamic representation of the turbo jet engine. The lack of an accurate dynamic plant model is the root cause of the problem since active feedback control of the engine cannot be implemented effectively with a low fidelity model. Thus,

the main project deliverable is a plant model, or a mathematical representation of the JetCat's dynamic nature.

Further, there is not currently a means of gathering the necessary thrust data required to develop a dynamic model. Figure 1.1 shows the current measurement apparatus used to measure the JetCat's thrust. The most detrimental feature of this thrust stand is that it has a set of linear rails that have friction, which must be overcome by the thrust generated from the JetCat. Rather than trying to account for the error in our dynamic measurements due to friction, a new thrust stand will be designed similar to that shown in Figure 1.2. This design uses a moment arm about a pivot, which could, for instance, be bearing with negligible friction, making the thrust stand much more suitable for transient data measurements.



Figure 1.1: JetCat thrust stand

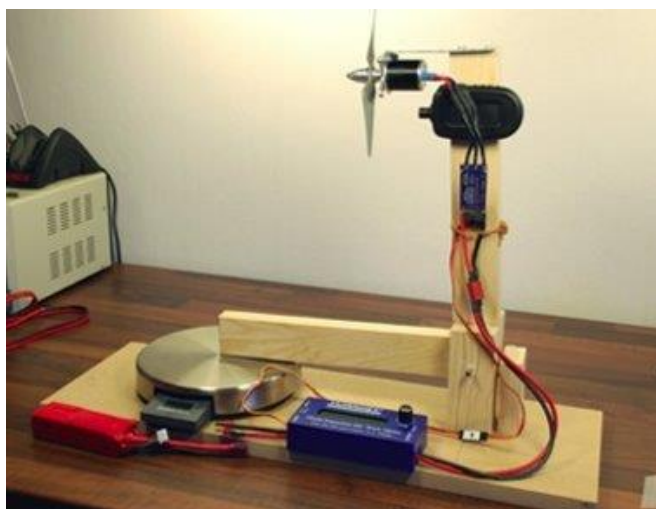


Figure 1.2: Moment Arm Thrust Stand

The users of the JetCat P180 dynamic model will be Dr. McCrink and possibly other researchers who focus on UAV controls and autonomy. Thus, the engine model desired to be formulated, which will likely be in the form of a Matlab/Simulink script, must contain well documented steps which are scientifically repeatable. The dynamic model created will be specific to the JetCat P180x, which previously powered the Avanti UAV and is projected to propel future ARC aircraft. However, with well documented steps of the presented measurement and modeling techniques, Dr. McCrink will be able to easily apply the team's methods to other micro turbo jet engines. Thus, this project is of value not only to the Avanti UAV, but also to other autonomous flight projects pursued by Dr. McCrink and other researches.

Secondary Research

After finalizing the problem definition related to controlling the JetCat P180, an initial literature review was conducted to research existing solutions for accurately modeling the transient nature of the turbojet. During this literature review, research papers related to turbine engines, micro-turbojets, and dynamic modeling techniques were studied in order to better understand the difficulties associated in simulating such a complex system. Summarized below are influential findings presented by secondary research sources, and how such theories and ideas could potentially affect stakeholders associated with the problem statement.

After conducting an in-depth literature review, it was concluded that very little research has been conducted on analyzing the transient nature of micro-turbojets [1, 8]. Most scientific papers related to micro-turbojets focus on the prediction of the steady-state performance of these gas turbines [1-5]. Researchers, such as Mattson, Gao et al, and Fozo et al, have previously experimented with JetCat P70 and P80 engines by comparing experimental thrust and pressure measurements to theoretical values predicted by thermodynamic and fluid dynamic principals. Although papers produced by these researchers do not provide insight into the transient nature of micro-turbojets, valuable knowledge was gained by learning what parameters are monitored during turbojet operations, such as turbine speed, fuel flow rate, and exhaust gas temperature. Additionally, the experimental set-ups utilized in previous research were presented, which lead to valuable insight regarding the test equipment required to investigate the dynamic response of the JetCat P180.

Although the majority of the research articles examined during the literature review focused on the steady-state performance of turbojet engines, one source was discovered that attempted to capture the dynamic nature of a JetCat P200. In their 2015 paper, Yang and Zhu used system identification techniques to experimentally formulate a transfer function relating engine RPM to a given throttle input. Their work resulted in a Linear Time Invariant (LTI) second-ordered transfer function that semi-accurately predicted the transient response of the P200 to different throttle inputs. Unfortunately, Dr. McCrink has previously utilized this model in past research and discovered that the model does not accurately characterize the throttle-RPM relationship under varying environmental conditions. By analyzing past flight test data, Dr. McCrink has theorized that the transfer function governing the throttle-RPM relationship at low throttle settings and airspeed conditions is of a different order or form than the mathematical function relating these two parameters at high throttle settings and airspeed.

The primary market for our model consists of Dr. McCrink, who would like to incorporate the developed plant model into unmanned aerial vehicles propelled by the P180 turbojet. As previously mentioned, there is a lack of robust dynamic models for micro-turbojets, and a true dearth of information on the relationship between throttle and thrust for JetCat engines. Thus, the greater research community stands to benefit from our findings and final model.

A plant model is useful in predicting a system's output for a given input, and is used to create a controllable system. The transfer function created in this capstone project is intended for use in a UAV control system, so a user (or computer) can adjust the throttle inputs to achieve its desired speed.

In the design of a plant model, there are several constraints to consider. The constraint of most importance to the team relates to the inputs and outputs to the plant model. The variables used has to consist of information that is attainable during testing. As such, the model is restricted to using the data that is gathered by an electrical control unit (ECU). To note, the ECU has more data available internally than the outputs it provides, so an electrical routine is required to access stored information. Available information collected via the ECU include fuel flow, RPM, and exhaust gas temperature.

A robust system of testing and validating the model is needed to address issues associated with the potential solution. Should a bad model be implemented in a control system, an aircraft can become unstable or uncontrollable and cause harm to its operators or by-standers. Reducing the likelihood of developing an inaccurate plant model is of utmost importance for vehicles implemented in situations with people involved.

Needs Chart

Based on the problem that is being solve, and looking at factors leading to the issue, there are many design needs. Moreover, the design process will apply to creating a model and test stand. The identified needs will be described below.

Accuracy: The accuracy of the model or test equipment is of the utmost importance. As has been noted before, the issue is the lack of an accurate model for transient models. Further, without an accurate model, a control system could not operate correctly, potentially leading to stability issues. For the test stand, a structure is needed to ensure accurate data collection. Different thrust stand designs can make it easier or more difficult to record accurate data from related sensor.

Ease of Experimentation: To be able to design and test the model in a reasonable amount of time, the model and experimental set-up needs to be easy to use. During winter months, the ability to test an engine in the wind tunnel is limited, as there are many graduate students utilizing this resource. Models need to be easy to test and validate, and thrust stands need to be easy to set-up with the JetCat engine.

Analytical Complexity: The choice of model and design of the thrust stand is important, and the complexity of running a model or building a stand should be taken into account. This factor affects the time required to create a model and analyze the physics of a test stand.

Cost: While cost of a system should be taken into account, the goal of this project is to design a system that will work as needed. The cost of the system regardless of our choices will come in below the provided budget.

Adaptability: Another need to consider is for the greater scientific and aerospace engineering community. To create a system that is applicable to more applications would of great benefit. For example, creating a methodology that extends to more engines and an adaptable thrust stand design would allow for characterization of more micro jet engines. However, the immediate problem does not require an adaptable procedure or system, and thus does not make adaptability a priority.

Table 1.1: Outline of Design Needs

Design Need	Weight
Accuracy of Model	5
Ease of Experimentation	4
Analytical Complexity	3
Cost	1
Adaptability	1

Based on these needs, two approaches to model creation and two test stand designs were compared. The scores are outlined below.

Table 1.2: Designs Scored

Design Elements	Design Decision	Weight	System ID	Analytical Derivation	Linear Stand	Moment Stand
Analytical Complexity	3	3		1	4	4
Accuracy of Model	5	5		4	2	4
Cost	1	2		5	5	3
Ease of Experimentation	4	3		3	4	5
Adaptability	1	4		1	3	3
Total		52		41	46	58

*1 = Low, 5 = High

From Table 1.2, the team decided to use the moment stand for the thrust stand design and system identification for determining the plant model of the engine.

Chapter 2 – Systems Design

Utilizing the scored designs from the problem definition, the team began the development of a thrust stand. In particular, a thrust stand utilizing a moment arm for thrust measurements was developed.

Development of Concepts

The critical considerations in the design of the thrust stand were the structural mechanics of the beams, the mounting of the JetCat, and the aerodynamics of the overall stand, each of which are discussed below.

Structural Concepts:

The concepts for the overall structure of the test stand resulted from researching general jet engine thrust stands, and brainstorming how to incorporate existing designs to this specific application utilizing a micro-turbojet. These potential designs are shown below in Figure 2.1, each of which employs the moment arm measurement technique as discussed above in the problem definition. The structure in concept 2.1 (a) is similar to the thrust stand located in Bolz Hall, however, it was adapted to incorporate a pivot point and moment arm. Concept 2.1 (b) is very similar, however, it employs 4 spread out vertical posts, which could reduce material used. In an effort to reduce structural twisting, as well as the complexity involved in using multiple vertical beams, concept (c) was developed which employs only one vertical beam.

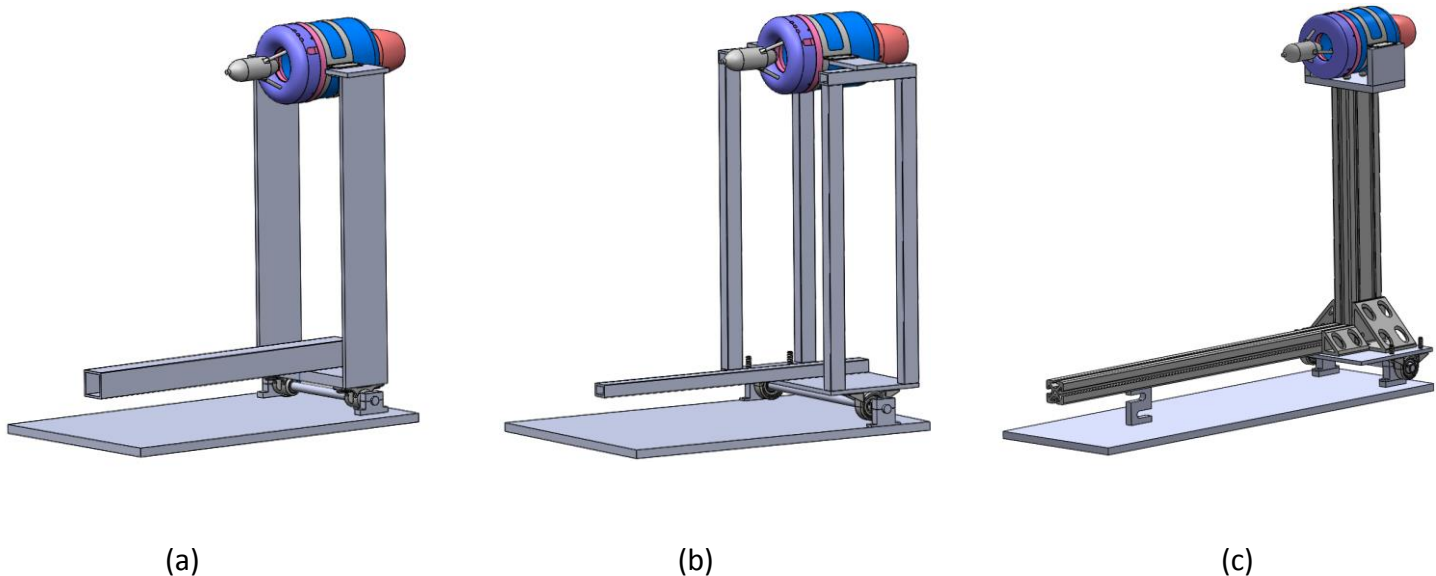


Figure 2.1: Thrust Stand Structural Concepts

Structural Concept Selection:

Design C was selected for further development based off the screening matrix shown below in Table 2.1. The first factor considered was torsional rigidity of the structure; with multiple beams supporting the frame, a moment could be created by vortex shedding which would negatively impact the load cell readings, which are crucial for the system identification. The aerodynamic profile criterion was used to judge how well the stand would fair in the wind tunnel. Design C was chosen as the highest rated potential design, not for its aerodynamic footprint, but rather, for the ease of implementing a fairing which could streamline the air flow. In addition, Design C utilized a single beam that reduced the number of parts required for the stand and complexity.

Table 2.1 Structural Design Screening

Criteria	Thrust Stand Concept		
	A	B	C
Torsional Rigidity	0	-	+
Aerodynamic Profile	0	-	+
Tolerance Stacking	0	-	+
Adaptability	+	+	0
Total +'s	1	1	3
Total -'s	0	3	0
Net	1	-2	3

Adapter Concepts:

The mounting clamp included with the JetCat does not allow for direct mounting to the thrust stand's vertical post, thus, a new mounting method was required. The 3 major mounting concepts considered are shown in Figure 2.2. The design in Figure 2.2a consists of an off the shelf clamp welded to a metal bracket, which would then bolt to the vertical beams. The designs featured in Figures 2.2(b) and Figure 2.2(c) both utilize the JetCat's original mounting clamp. The adapter in Figure 2.2(b) would consist of one U-shaped mounting block, while the design shown in Figure 2.2(c) would consist of 3 assembled rectangular blocks.

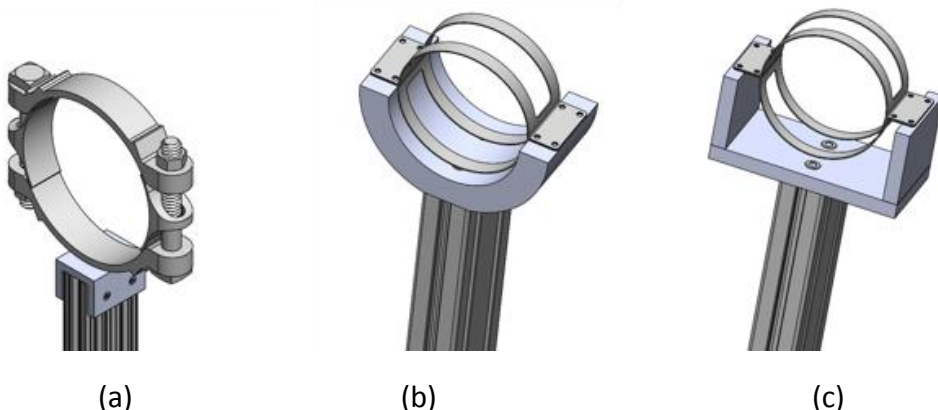


Figure 2.2: Adapter Design Concepts

A similar selection process was used to determine the design that encapsulated the criteria desired. Design C excelled in the adaptability criteria due to the larger adapter frame which could accommodate larger engines in future projects. In addition, Design C was appealing and scored higher due to the cost associated with manufacturing the part. Lastly, the aerodynamic footprint was similar to the others. Additionally, Design C allows for airfoil to surround the bottom half of the engine during dynamic testing, which results in better heat transfer and cooling characteristics. With Design 3 outscoring the other designs, it was clear that this concept should be implemented in the thrust stand.

Table 2.2 Adapter Designs Scored

Criteria	Weight	Concept A	Concept B	Concept C
Adaptability	3	5	1	4
Cost	5	3	1	4
Ease of Manufacturability	4	2	2	4
Aerodynamic Profile	2	4	4	4
Total		46	24	56

Airfoil Design

To reduce vortex shedding behind the vertical post, an airfoil will be wrapped around the beam as shown in Figure 2.3. The airfoil's considered included the NACA 0012 and NACA 0024, which, when sized to enclose the beam, have the physical characteristics listed below in Table 2.3.

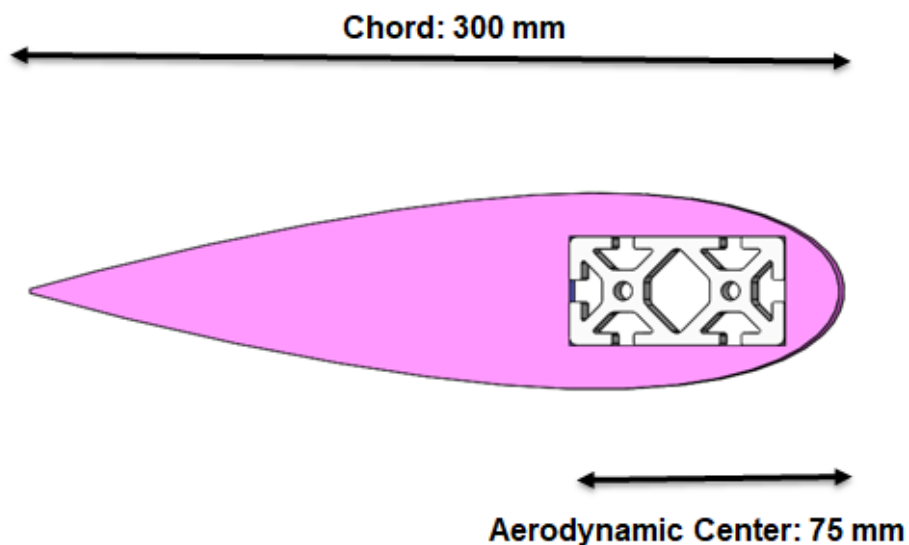


Figure 2.3 Airfoil Design

The decision to choose the NACA 0024 over the NACA 0012 came from multiple factors as shown in Tables 2.3 and 2.4. The chord length was the most influential factor when comparing the two designs; the 0.45-meter chord length of the NACA 0012 fairing was disproportionately too large for the 3' by 5' wind tunnel, and it was deemed that a shorter airfoil should be used despite the larger coefficient of drag. Per Dr. McCrink's suggestion, a modified NACA 0024 profile will be implemented with a smaller width, as compared to the one shown above. This modified fairing will streamline only the leading edge and trailing edge of the vertical post; no fairing material will be present on the sides of the beam.

Table 2.3: Airfoil Designs Considered

	NACA 0012	NACA 0024
Price	—	—
Coefficient of Drag	—	20% higher
Chord Length	0.45 m	0.30 m
Area	0.21 m	0.14 m
Weight	152.49 g	131.73 g

Airfoil Selection

Table 2.4: Airfoil Screening Matrix

Criteria	Weight	NACA 0012	NACA 0024
Coefficient of Drag	4	5	4
Chord Length	5	3	4
Area	3	2	3
Weight	2	3	4
Total	--	44	49

Description of Selected Concept and Rationale

The overall design concept incorporates the selected structural, mounting adapter, and airfoil designs described in previous sections. Figure 2.4 (below) shows the final thrust stand concept that incorporates each of these subsystems. Figure 2.4 (a) shows that the horizontal beam is 33% longer than the vertical beam in order reduce the load cell force and ensure the load cell does not go over loading capacity. The vertical beam length was chosen so that the JetCat will be positioned roughly in the center of the wind tunnel. With this length assumption, beam cross sections were sized as shown in following sections.

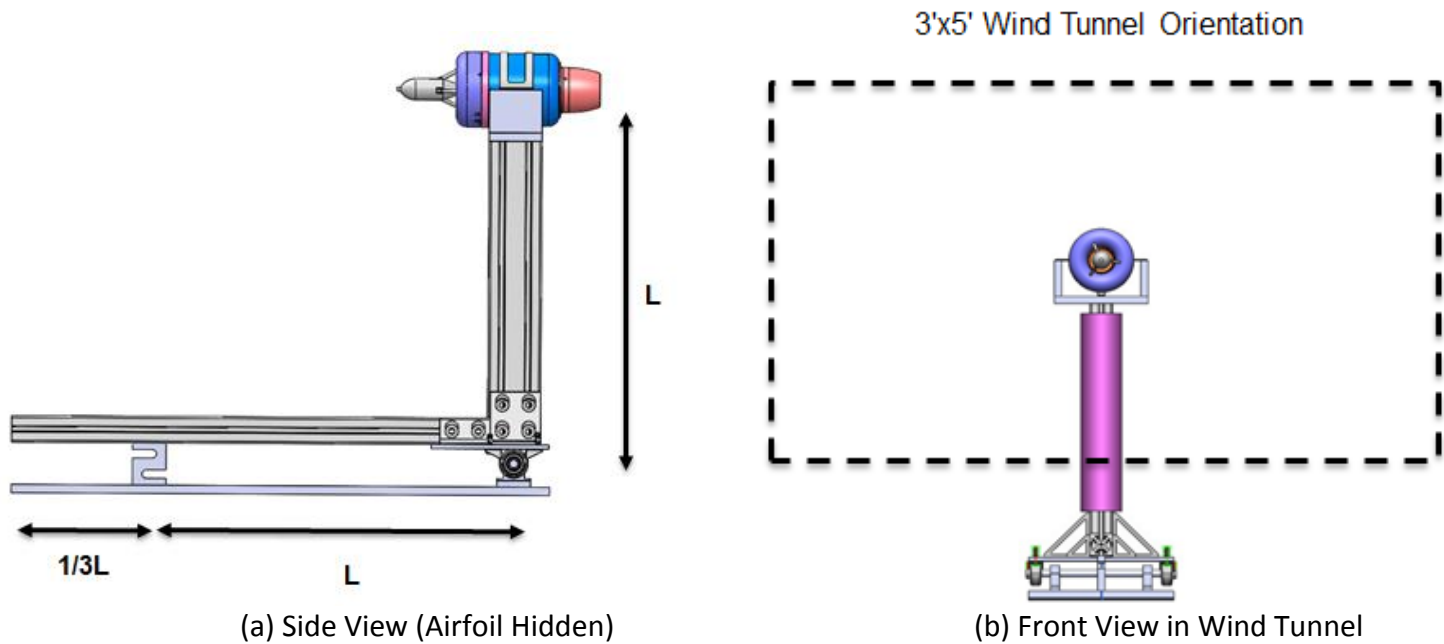


Figure 2.4 Overall Design of Thrust Stand

Identify Metrics and Requirements

Based on the knowledge gained in creating and selecting a concept, the team created an updated needs matrix (shown below). In particular, the team found that the structural rigidity and ease of manufacture to be of more importance than previously believed.

Table 2.5: Measurable Metrics for each Need

Design Need	Rank (5 is most important)
Structural Rigidity	5
Ease of Manufacture	3
Accuracy of Model	5
Ease of Experimentation	3
Analytical Complexity	3
Cost	1
Adaptability	1

Based on the design needs, measurable metrics were noted, along with the desired value ranges (Tables 2.6 and 2.7).

Table 2.6: Measurable Metrics for each Need

Design Need	Measurable Metric
Structural Rigidity	Stress values, Displacement magnitude, Natural frequency
Ease of Manufacture	Estimated manufacturing time (days)
Accuracy of Model	System uncertainty (N)
Ease of Experimentation	Estimated stand set-up time (min.)
Analytical Complexity	Time to derive model (days)
Cost	US Dollars (\$)
Adaptability	Quantity of different engine models that can fit (#)

The metrics listed for each design need will be discussed individually below.

Stress Values: Because of the volatile nature of the engine during operation, the safety factor for stress needs to be large enough to ensure the stand does not experience mechanical failure. Mechanical failure would be catastrophic to the test stand and wind tunnel, making the safety factor a major concern.

Displacement Magnitude: Displacement of the beam directly affects the load cell reading. The higher the displacement, the lower the accuracy of the readout. As the geometries are altered sufficiently due to excess load or a poorly designed stand, the load cell readout is rendered defective and cannot be used to accurately model the engine. Displacement should be minimized.

Natural Frequency: Triggering resonant structural modes would prove to be catastrophic and a significant safety issue. For this reason, the natural frequency of the selected beam should be much higher than the frequency associated with any vibrational forcing functions experienced during data collection trials.

Estimated Manufacturing Time: In the selection between designs, the estimated manufacturing time should also be considered. The lower time needed to manufacture a design will aid the team in later efforts, such as allowing more time to perform tests and collect data. Moreover, the ease in manufacturing would allow for quicker iteration in stand design, should the need arise.

System Uncertainty: Accuracy of the data is of the utmost importance, as this directly affects the accuracy of the plant model obtained through experimentation. An effective controller cannot be designed based off of the modeling of an inaccurate plant model. Mechanical and electrical designs with the least amount of uncertainty will be prioritized.

Estimated Stand Set-Up Time: As many tests at varying airspeeds need to be conducted, the stand set-up time should be considered. To make the most efficient use of the team's time at the ARC, a stand with a quick set-up is preferable.

Time to Derive Model: To further separate the varied designs based on their complexity, the time needed to derive physics models for each design was considered. Specifically, a complex design requires static force balances at each load bearing member, complicating stress and deflection analysis. Simpler stands require fewer force balances and are optimal for time considerations.

Cost: The team needs to stay under a budget of \$3500, so cost of test stand materials is required to be examined. Ideally, the stand will not take up a large portion of the budget, leaving ample room for more expensive electrical equipment the team may need down the road.

Quantity of Compatible Engine Models: Dr. McCrink would like to use the test stand down the road to test different engines. The stand should be designed to be adaptable and strong enough to be used for engines of similar geometric size.

Table 2.7. Desired Metric Value and Acceptable Ranges

Metric	Unit	Desired Value	Acceptable Range
Stress Value	Safety Factor	> 10	≥ 4
Displacement Magnitude	mm	0	≤ 1.3
Natural Frequency	Hz	>> 8 Hz	$> 8 \text{ Hz}$
Estimated Manufacturing Time	Days	1	≤ 3
System Uncertainty	N	0.01	≤ 0.1
Set-Up Time (est.)	Minutes	20	≤ 45
Derivation Time (est.)	Days	≤ 14	≤ 31
Cost	US Dollars	\$0	$\leq \$1,500$
# of Compatible Engine Models	#	≥ 3	≥ 1

Design Development

As discussed above in *Identifying Metrics and Requirements*, the stress values, displacement magnitudes, and characteristic natural frequencies of the thrust stand's structural elements are of great importance to the overall success of the project as the accuracy of collected data and safety of the experimental procedure is directly affected by these design requirements. In the following section, the engineering models, mathematical formulas, and resulting metric values associated with the thrust stand design are presented.

Although the thrust stand is comprised of several different discrete pieces, the most critical part of the overall design is the vertical beam that is responsible for restraining the Jetcat while conducting engine trials. In order to ensure that the vertical post is designed safely and to a quality that meets the requirements stated in the needs matrix, the resulting stress and displacement values were calculated for a variety of beam cross sectional geometries. Additionally, the natural frequency of the vertical post was computed for several different cross-sectional geometries as to ensure that aerodynamic effects would not excite vibrational modes within the thrust stand's structure.

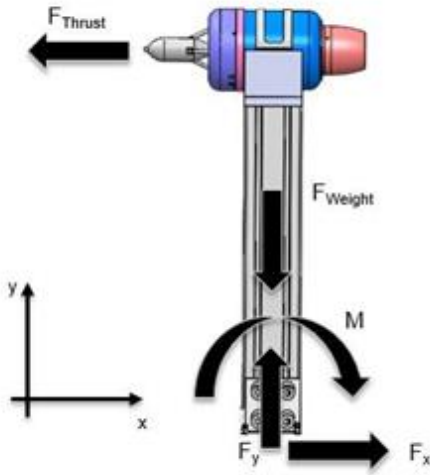


Figure 2.5: Free Body Diagram of Vertical Beam

Shown above in Figure 2.5 is the Free Body Diagram (FBD) of the thrust stand's vertical post. Since the vertical post was designed for the most critical loading condition, it was assumed that stress and displacement values would be largest when the engine operates at its maximum power and zero airspeed. This loading condition was assumed to be the most critical test point since engine thrust and aerodynamic drag act in opposite directions along the x-axis. If air drag was to act upon the vertical beam, it would oppose the engine's thrust, resulting in a lower net force along the x-direction, which further cascades to smaller stress and displacement values. Additionally, the vertical beam was subjected to the combined weight of the Jetcat P180 as well as the beam itself. In Figure 2.5 above, engine thrust is represented by F_{Thrust} while the combined weight of the vertical beam and Jetcat P180 is denoted by F_{Weight} . Lastly, since the vertical post was modeled as a cantilever beam, two reaction forces and a reaction moment are responsible for supporting the beam and are denoted by F_x , F_y , and M , respectively.

Shown below in Figure 2.6 is the shear-moment diagram representing the distribution of forces and moments along the height of the vertical post. This diagram was created via *SkyCiv* software, a cloud-based, mechanics of materials program which computes support reactions in addition to shear-moment diagrams for beam-based structures. By referencing Figure 2.6, it can be noted that the maximum shear force and internal moment exerted upon the vertical post occurs at the base of the beam at $y=0$ meters. Note that although the shear-moment diagram depicted in figure 2.6 is specific to the final thrust stand design, the general trend that internal shear and moment reaches maximum values at the beam's base remain valid for all cantilever designs loaded in the configuration shown in figure 2.5.

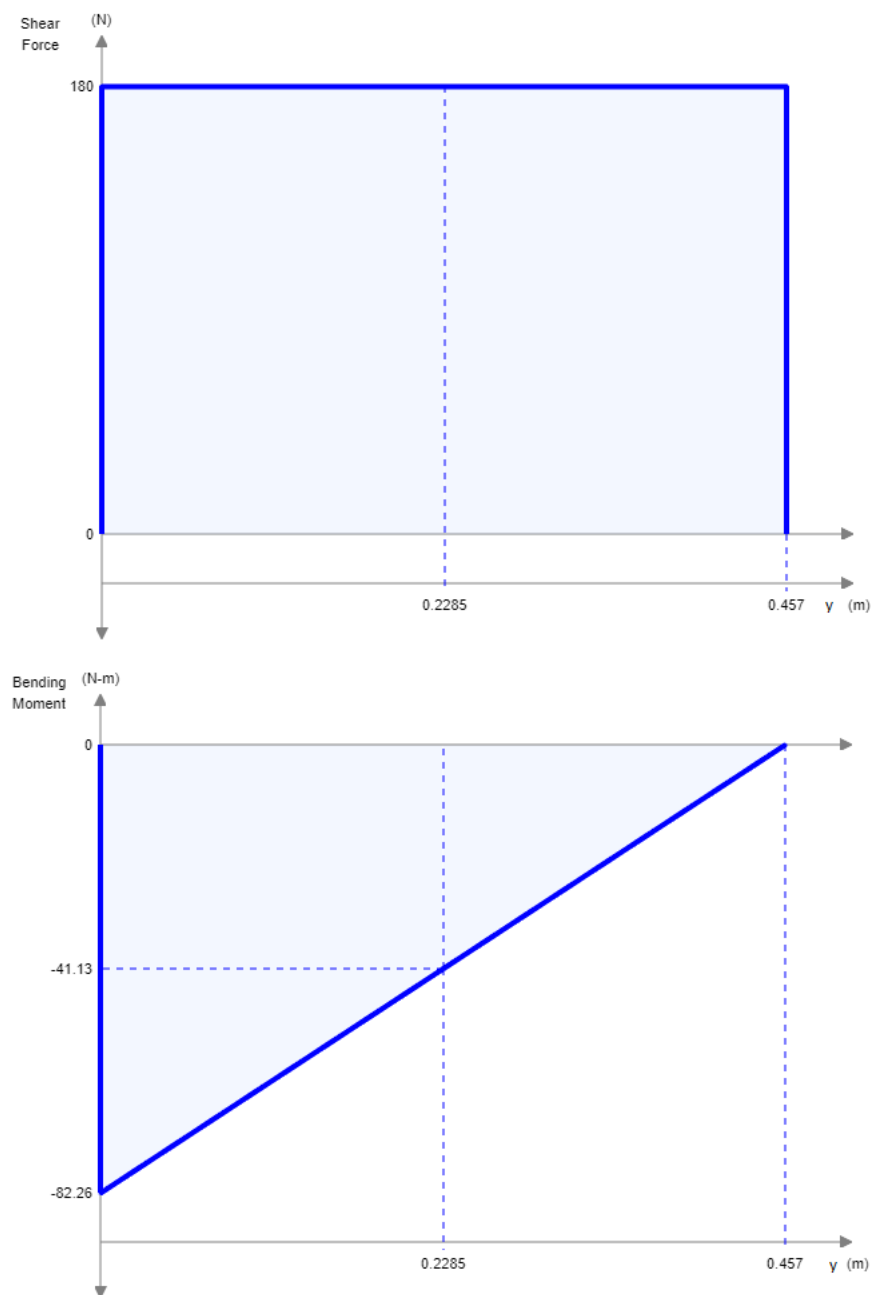


Figure 2.6: Shear-Moment Diagram of Vertical Beam

Since the vertical beam is supported via two reactionary forces and a supportive moment, there are three modes of loading that contribute to stress build-up in the vertical post's base. These three modes of loading include bending due to the support moment M , a normal stress associated with the axial force F_y , and a shear stress from the support force F_x . A visualization of the forces and moment concentrated at the beam's base is provided below in Figure 2.7.

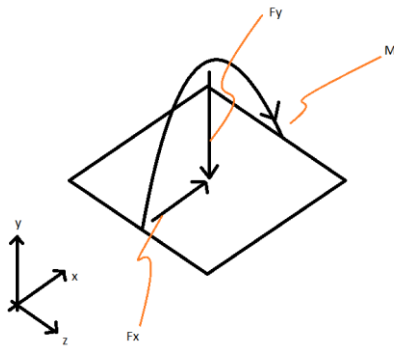


Figure 2.7: Visualization of the Loading Modes Located at Beam's Base

Equation 1 shown below was utilized to compute the amount of normal stress generated at the vertical beam's base due to the beam bending. In Equation 1, σ_B represents the normal stress resulting from bending, M corresponds to the reactionary moment subjected to the beam's base, C is the distance from the beam's neutral axis to its perimeter, and I denotes the beam's area moment of inertia.

$$\sigma_B = \frac{M*C}{I} \quad (1)$$

After computing the normal stress resulting from beam bending, Equation 2 was used to calculate the magnitude of normal stress due to axial loading. As shown below in Equation 2, σ_A represents the normal stress due to axial loading, F_y corresponds to the vertical support force at the base, and A corresponds to the cross-sectional area of the vertical beam.

$$\sigma_A = \frac{F_y}{A} \quad (2)$$

Since the bending stress computed in Equation 1 and axial stress calculated via Equation 2 are both classified as normal stresses, the net normal stress at the beam's critical point will correspond to the sum of these two values. Equation 3 allows for the computation of the maximum equivalent normal stress at the beam's critical point, σ_N , by adding the bending normal stress, σ_B , calculated in Equation 1 to the axial normal stress, σ_A , determined via Equation 2.

$$\sigma_N = \sigma_B + \sigma_A \quad (3)$$

In addition to the normal stresses computed via Equation 1 and Equation 2, the beam's base is subjected to a shear stress resulting from the support force acting in the x-direction. Equation 4 listed below allows for the computation of the average shear force, τ , in terms of the support force acting in the x-direction, F_x , and cross-sectional area of the beam, A .

$$\tau = \frac{F_x}{A} \quad (4)$$

As depicted in figure 2.7 and suggested by Equations 1, 2, and 4, the beam's critical point is subjected to both normal stress as well as shear stress. Von Mises theory was utilized in order to calculate an equivalent stress value which combines the effects of normal loading and shear loading. Equation 5 listed below is an abbreviated form of von Mises theory utilized for 2-D stress analysis, where σ_{EQ} represents the equivalent stress resulting from a normal stress, σ_N , and shear stress, τ .

$$\sigma_{EQ} = \sqrt{\sigma_N^2 + 3\tau^2} \quad (5)$$

After computing an equivalent stress, σ_{EQ} , via Equation 5, the beam's safety factor was calculated by utilizing Equation 6, where σ_{Yield} corresponds to the yield strength of the vertical post.

$$\text{Safety Factor} = \frac{\sigma_{Yield}}{\sigma_{EQ}} \quad (6)$$

In addition to analyzing the vertical post's safety factor based on stress analysis, the amount of displacement the cantilever beam's free end would experience under the critical loading condition was also investigated. Although the vertical post experiences external forces in both the x and y direction, only the engine's thrust force would cause lateral displacement of the cantilever's free end. Shown below in figure 2.8 is a diagram depicting the lateral displacement of a cantilever beam subjected to a point load at its free end. Note that figure 2.8 is provided by Ruina [6].

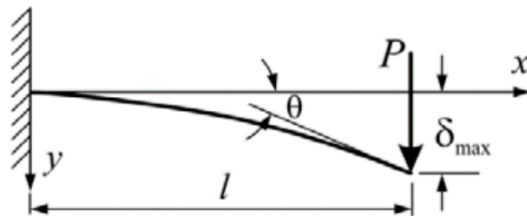


Figure 2.8: Visualization of Cantilever Beam Bending

Ruina not only provided Figure 2.8, but also presented a formula which allowed for the computation of how much lateral deflection a cantilever beam's free end experiences due to a localized point load. Equation 7 listed below computes the resulting lateral displacement, δ_{max} , caused by a point load of magnitude P . Note that in Equation 7, L represented the length of the beam, I corresponds to the beam's area moment of inertia, and E denotes the beam's Young's Modulus.

$$\delta_{max} = \frac{P * L^3}{3 * E * I} \quad (7)$$

Upon substitution of appropriate variables, Equation 7 was modified into Equation 8, where variables P and L were replaced by the thrust of the Jetcat P180, F_{Thrust} , and height of the vertical post, H , respectively.

$$\delta_{max} = \frac{F_{Thrust} * H^3}{3 * E * I} \quad (8)$$

After computing the amount of lateral displacement the cantilever beam would experience under the critical test condition, vibrational effects were examined in order to ensure that the thrust stand's structural vibrational modes would not be excited during data collection trials. It was assumed that aerodynamic effects, such as vortex shedding, would be the primary forcing functions that could potentially lead to structural resonance within the thrust stand. In order to minimize the effects of vortex shedding, it was concluded that encapsulating the vertical beam of the thrust stand with an airfoil shaped fairing would be beneficial. By wrapping the vertical beam in a streamlined shape, vortex shedding caused by the blunt profile of a rectangular beam would be effectively reduced. Although vortex shedding caused by the beam's profile was minimized via the airfoil fairing, vortex shedding produced by the engine's nacelle's geometry could not be altered. Instead, it was concluded that the vertical beam's natural frequency had to be much greater than the frequency associated with the engine's vortex shedding. The following paragraphs outline the equations used to estimate the beam's natural frequency as well as the frequency of vortex shedding.

In order to estimate the frequency of the aerodynamic forcing function, research was conducted regarding the vortex shedding associated with the Jetcat engine. It was assumed that the external geometry of the Jetcat P180 could be modeled as a rectangular cylinder. By utilizing this assumption in combination with Equation 9 below, the frequency of vortex shedding could be estimated. In Equation 9, S_T denotes the experiential Strouhal number, f represents the frequency of vortex shedding, L is the characteristic length of the shape in question, and U corresponds to the freestream velocity of the surrounding fluid.

$$S_T = \frac{f * L}{U} \quad (9)$$

Since the Jetcat was modeled as a rectangular cylinder, the characteristic length corresponds to the engine's diameter (112 cm) and the Strouhal number has a value of 0.13, as experimentally determined by Schewe [7]. Additionally, by algebraically rearranging Equation 9, it can be concluded that the vortex shedding frequency is directly proportional to the freestream velocity, which means that the maximum forcing frequency will occur at the maximum wind tunnel velocity of 100 mph, or 45 m/s. By substituting these numerical values into Equation 9, it can be concluded that the thrust stand will be subjected to a forcing function with a maximum frequency of 8 Hz.

After computing the maximum frequency of the aerodynamic forcing function as shown above in Equation 9, the natural frequency of the vertical post was computed for a variety of cross-

sectional geometries. Equation 10 shown below was utilized to calculate the natural frequency, ω_N , of a cantilever beam, where E denotes the Young's Modulus, I represents the area moment of inertia, M corresponds to the mass of the beam, and H is the length of the vertical post. It was crucial to ensure that the natural frequency of the vertical post was much greater than the frequency associated with vortex shedding as to safeguard the thrust stand from being subjected to oscillatory forces that could result in structural resonance.

$$\omega_N = 1.875^2 \sqrt{\frac{E*I}{M*H^3}} \quad (10)$$

Table 2.8 presented below summarizes the results associated with the stress values, displacement magnitudes, and natural frequencies that correspond to a variety of beam geometries subjected to the critical test condition previously described. Note that only commercially available, discrete beam sizes were analyzed for the vertical post in an effort to minimize costs. Additionally, T-slotted aluminum extrusions, commonly referred to as 80-20, were only selected for analysis as these profiles would result in easy thrust stand manufacturing.

Table 2.8: Mechanical and Loading Properties of Vertical Beam Designs

Part Number	Width (mm)	Thickness (mm)	Stress (Mpa)	Safety Factor	Lateral Displacement (mm)	Natural Frequency (Hz)
30-6060	60	60	6.74	35.8	0.222	85.17
40-4040	40	40	11.82	20.4	0.585	54.80
40-4040-Lite	40	40	17.31	13.9	0.858	52.05
40-4040-UL	40	40	18.71	12.9	0.926	53.72
40-4080	80	40	3.35	72.0	0.083	110.13
40-4080-Lite	80	40	4.54	53.0	0.112	104.53
40-4080-UL	80	40	5.18	46.6	0.128	110.79
40-4012	120	40	1.61	149.6	0.026	163.08

As noted above in Table 2.8, it was decided to select Part Number 40-4080 for the vertical beam application. This aluminum extrusion, which has external dimensions of 80 mm by 40 mm, offers a very high safety factor of 72. Additionally, the free end of the vertical post experiences under 0.1 mm of lateral deflection, which is superior to the minimum deflection requirements of 1.3 mm. Additionally, the natural frequency of the vertical post constructed from this cross-sectional geometry is 110 Hz, which is much larger than the 8 Hz forcing function generated via vortex shedding.

In addition to analyzing the vertical post, the critical stresses, safety factor, and vertical deflection associated with the thrust stand's horizontal beam was also investigated. Although not as critical to the stand's overall safety as the vertical post, the horizontal beam is responsible for transferring the thrust-generated moment to a support force measured by the load cell. In order to ensure accurate thrust measurements are collected, it is necessary to design the horizontal beam to experience the minimal amount of deflection as possible.

Shown below in Figure 2.9 is the Free Body Diagram of the Thrust Stand's horizontal beam. Note that this structural element was modeled as a simply supported beam subjected to both an applied moment and point force corresponding to the beam's intrinsic weight. Since neither the load cell nor pivoting-support produce a reactionary moment, the beam is only supported by these elements' reactionary forces, denoted by $F_{Load\ Cell}$ and F_{Hinge} , respectively. Additionally, M denotes the applied moment and corresponds to the support reaction resulting from the Jetcat's thrust, as discussed in the design of the vertical post.

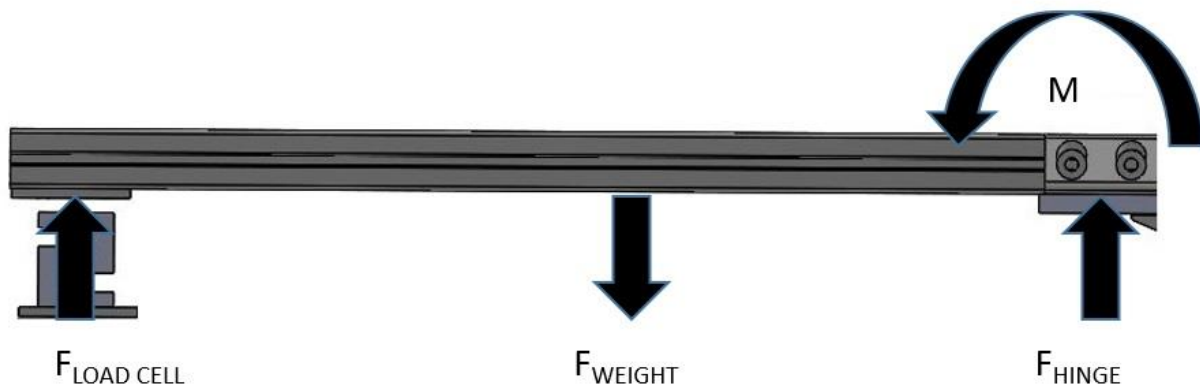


Figure 2.9: Free Body Diagram of Horizontal Beam

By utilizing the Free Body Diagram shown above in Figure 2.9 in combination with *SkyCiv* software, the horizontal beam's Shear-Moment diagram was produced, as depicted below in Figure 2.10. The shear-moment diagram presents crucial information such as the magnitude and location of an element's maximum internal shear force and bending moment. By referencing Figure 2.10, it can be concluded that the horizontal beam experiences its maximum internal moment at the hinged support and maximum internal shear force at the loadcell's position. After assuming that the relatively long beam would experience failure resulting from the internal moment before the internal shear force, it was concluded that the horizontal beam's critical point corresponds to the hinged location. Note that although the Shear-Moment diagram presented below in Figure 2.10 is specific to the horizontal beam's final design, the general trends regarding internal loads remained valid for all cross-sectional geometries analyzed.

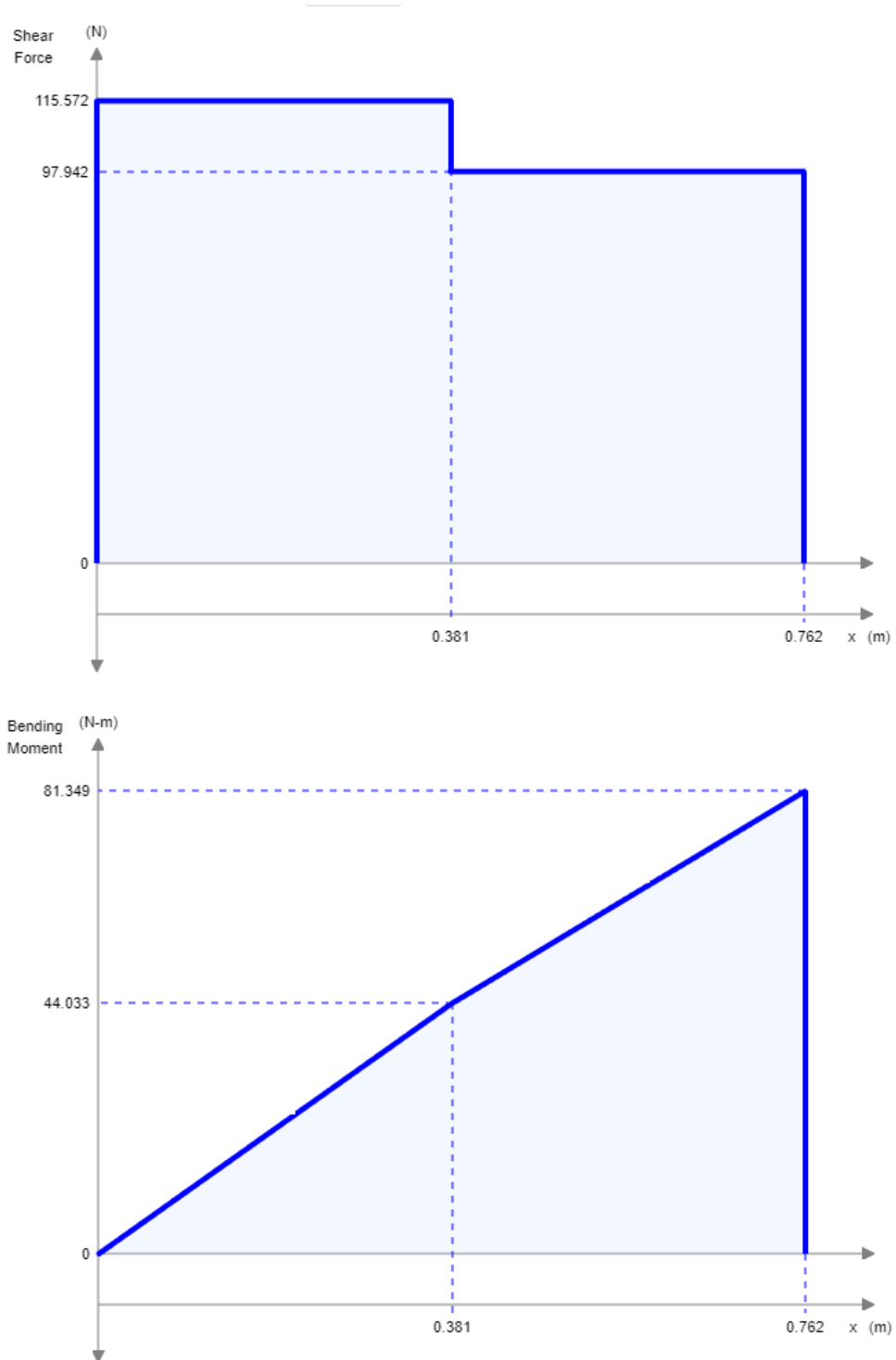


Figure 2.10: Shear-Moment Diagram of Horizontal Beam

After producing the Shear-Moment diagram depicted above and identifying the horizontal beam's critical point, a stress analysis was performed on the structural element. The same procedure outlined in Equations 1 through Equation 6 was applied to the horizontal beam's analyses. Note that the only difference between the stress analysis performed on the vertical beam and horizontal beam was that the horizontal beam did not experience normal axial loading, as analyzed via Equation 2.

In addition to performing a stress analysis on the horizontal beam, the amount of vertical deflection experienced by this structural member under the critical loading condition was also investigated. As visualized by the Free Body Diagram presented above in Figure 2.9, the horizontal beam is subjected to both an external moment and point force resulting from the member's intrinsic mass. Since the beam deflection equations presented below in Equation 11 and Equation 12 are valid for only one specific loading condition, the principle of superposition was assumed to remain valid in order to estimate the net deflection resulting from the two forms of loading.

Presented below in Equation 11 is the formula utilized to compute the amount of vertical deflection experienced by the horizontal beam resulting from the structural member's intrinsic mass. In general, Equation 11 is utilized to compute a beam's vertical displacement due to a point load located at the middle of the element being analyzed. For the specific case of the horizontal beam, F represents the total weight of the horizontal beam, L denotes the overall length of the beam, I corresponds to the beam's area moment of inertia, E symbolizes Young's Modulus, and X is an arbitrary position along the structural element's length.

$$\delta_1 = \frac{(F)(x)(3L^2 - 4x^2)}{(48)(L)(E)(I)}$$

In order to compute the horizontal beam's deflection due to the applied moment, Equation 12 shown below was used. In Equation 12, M represents the applied moment, L corresponds to the overall length of the beam, I is the beam's area moment of inertia, E symbolizes Young's Modulus, and X is an arbitrary position along the structural element's length.

$$\delta_2 = \frac{(M)(L)(x)}{(6)(E)(I)} \left(1 - \frac{x^2}{L^2}\right)$$

After computing the amount of deflection resulting from each case of loading subjected upon the beam, Equation 13 was utilized to calculate the net deflection of the horizontal beam. The validity of Equation 13 is reliant upon the horizontal beam experiencing a small amount of deflection as to ensure that the principle of superposition can be used. In Equation 13, δ_1 and δ_2 are calculated via Equation 11 and Equation 12.

$$\delta_{TOTAL} = \delta_1 + \delta_2$$

Shown below in Table 2.9 is a summary of the resulting critical stresses, safety factors, and amounts of vertical deflection corresponding to different horizontal beam designs. As with the vertical post, commercially available, T-slotted, aluminum extrusions were selected for analysis as they are proven to be relatively inexpensive and easy to work with. Note that in Table 2.9, the critical stress is presented in Mega-Pascal (MPa) and vertical deflections is shown in millimeters (mm).

Table 2.9: Mechanical and Loading Properties of Horizontal Beam Designs

Part Number	Width (mm)	Thickness (mm)	Stress (Mpa)	Safety Factor	Lateral Displacement (mm)
20-2020	20	20	119.18	2.02	6.232
20-2040	40	20	35.90	6.72	0.930
20-4040	40	40	20.76	11.61	0.521
40-4040	40	40	11.80	20.43	0.291
40-4040-Lite	40	40	17.31	13.94	0.435
40-4040-UL	40	40	18.69	12.90	0.473

As presented in Table 2.9 above, Part Number 40-4040 was ultimately selected for use in the horizontal beam application. This profile measures 40 mm in width as well as thickness. As a result, the horizontal beam experiences a maximum von Mises stress value of 11.8 MPa under the critical loading condition, corresponding to a safety factor of 20.4. Additionally, it is expected that the horizontal beam will only experience a vertical deflection of 0.29 mm, thus meeting the deflection requirement.

Bolting calculations were performed to ensure the current JetCat engine would not cause failure of the fasteners, as well as see what max thrust the bolts can withstand if a larger engine is used with the stand. Four bolting groups that support the load bearing components of the stand were selected for analysis and can be seen below.

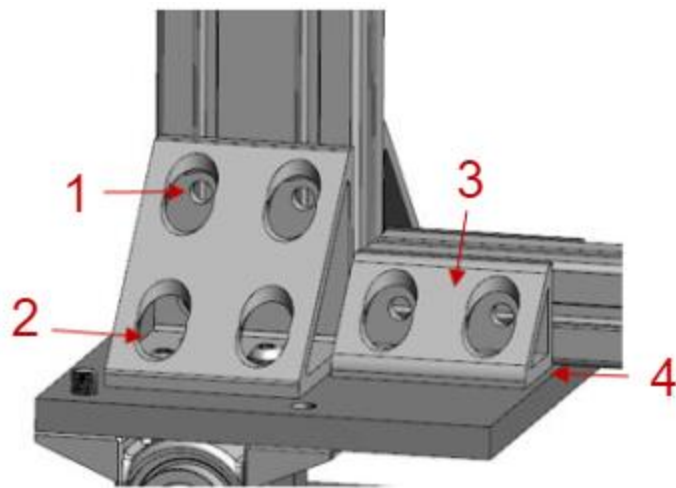
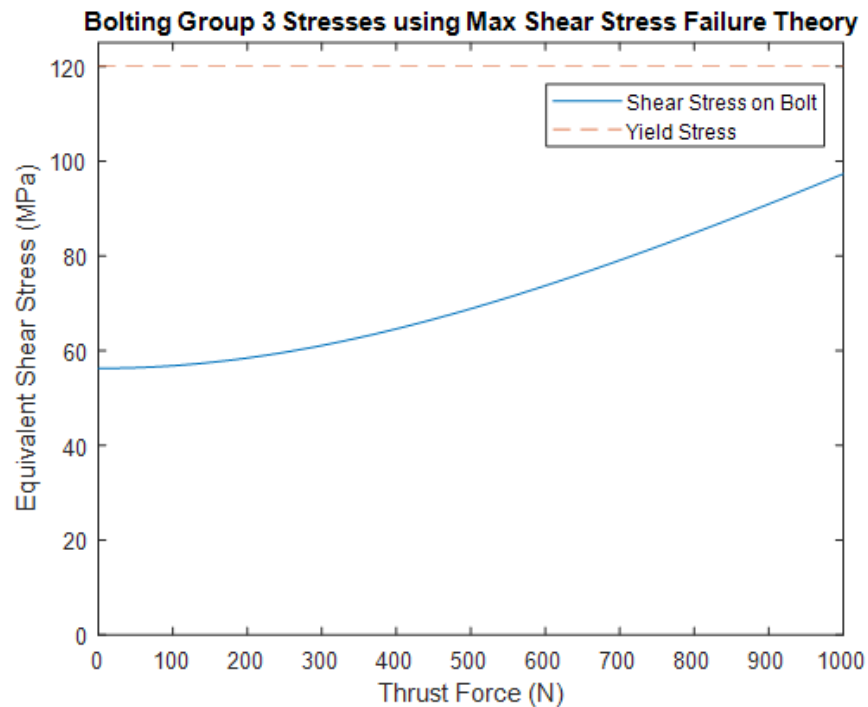


Figure 2.11: Bolting groups selected for failure analysis.

Methods determining the principal stresses within critical bolts of each group can be seen in Figure A.5 in the Appendix. Maximum shear stress failure was used to give the most conservative safety factors for the stand. It was determined that bolt group 3 had the most critical bolt, yielding at a thrust force of 300 lbs. This value is much higher than the expected force of 40 lbs, and allows for larger engines to be used on the stand. It should be noted that yielding was used for safety factor calculations, and ultimate strength of the bolt could be used to get a less conservative, more realistic value. Figures of stress versus thrust force and safety factor for bolt group 3 can be seen below.



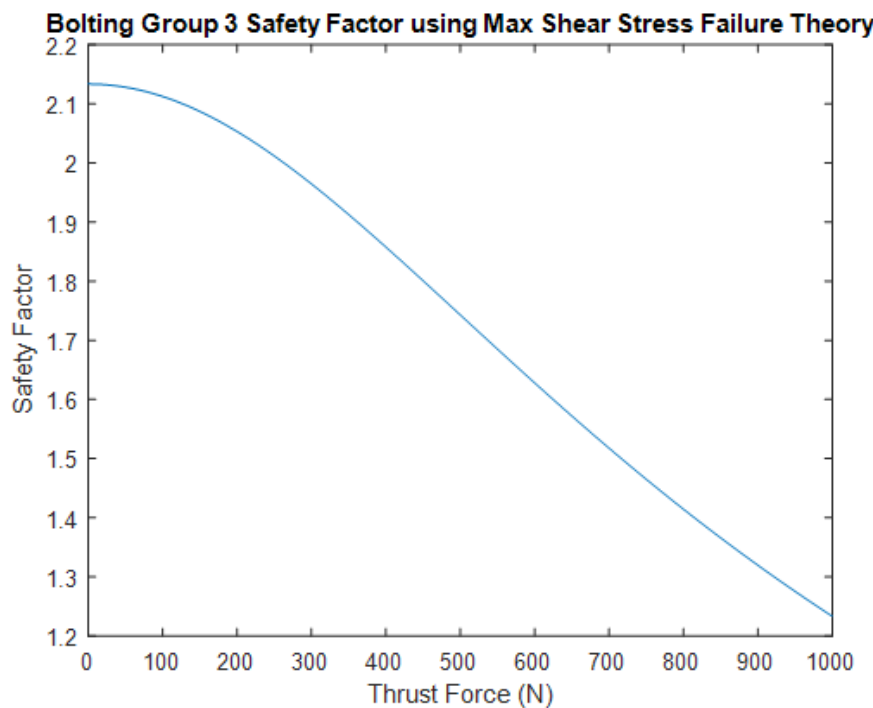


Figure 2.12: Bolting stress values and safety factors for range of thrusts.

The rest of the figures for bolt groups 2 through 4 can be seen in Figures A.6 and A.7 in the Appendix. From this analysis, the bolting groups are sufficient for the JetCat P180x as well as larger engines.

Chapter 3 – Detail Design

Development of Detail Design

The following details have been added to the thrust stand design since the Preliminary Design Review, based on feedback from our sponsor and advisor. Details of this sponsor feedback are also discussed in a later section.

- 1.) Adapted the test stand to be easily mounted to and removed from the 3'x5' wind tunnel. This is the function of the 1.5-inch shaft mounted to the underside of our test stand shown in figure 3.1. This shaft mounts to a clamp which is already installed in the beta table beneath the wind tunnel.
- 2.) Split the airfoil into sections which reduced its size considerably. This airfoil will be cut from foam, and then wrapped in reflective tape to prevent the airfoil from melting due to high temperature exhaust gas. The test stand position in the wind tunnel can be seen in figure 3.2, which shows that the airfoil section will protrude from the top of the wind tunnel floor board. Based on discussion with Dr. Rick Freuler this floor board must be cut so that it does not interfere with the test stand, while also ensuring minimal pressure losses due to leakage.
- 3.) Vertical support beam is mounted at the end of the test stand nearest to the load cell and will rest on the floor underneath the load cell. This adds structural support and reduces the possibility of deflection which could lead to inaccuracies in load cell measurement.

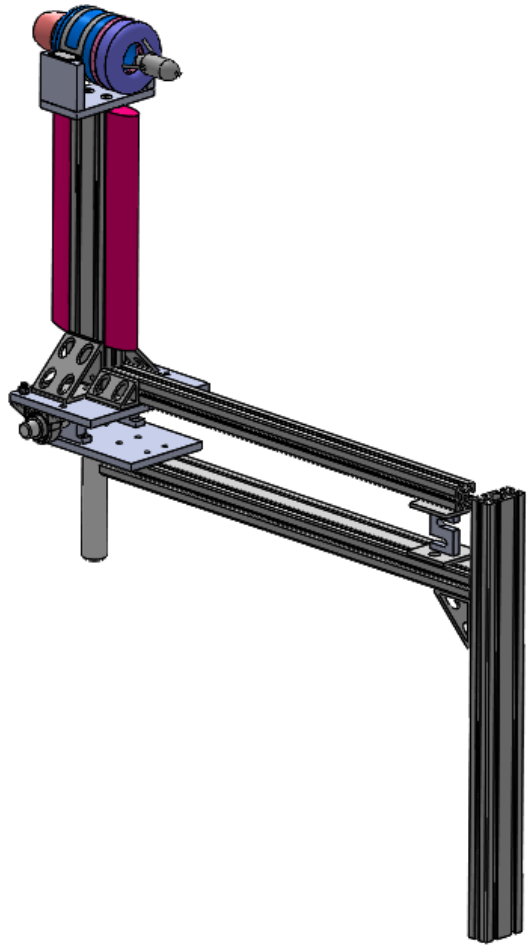


Figure 3.1 3D View of Final Thrust Stand Design

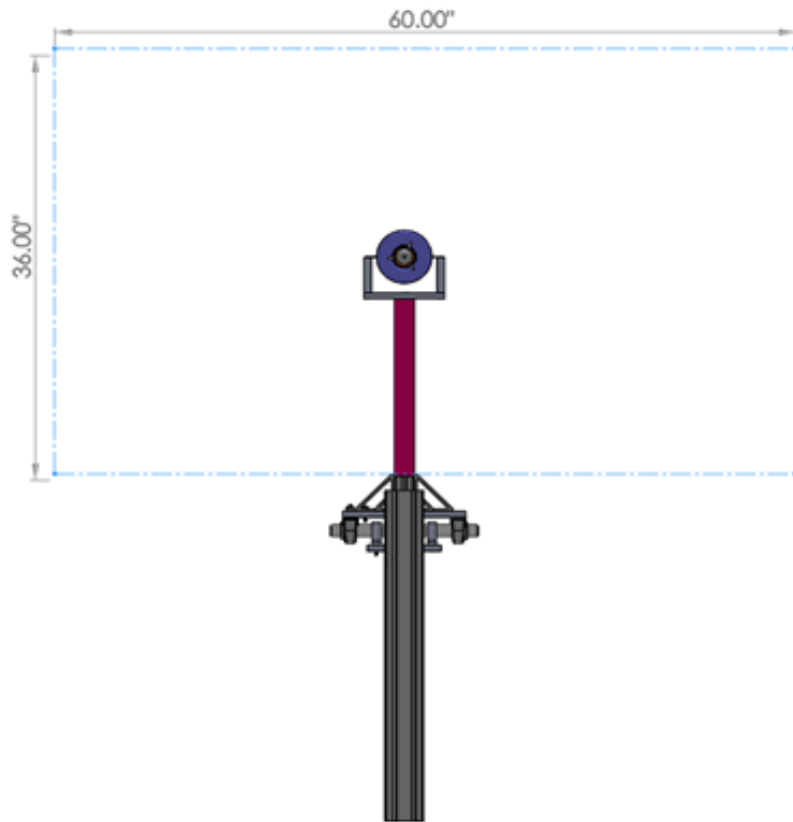


Figure 3.2 Front View of Final Thrust Stand Design

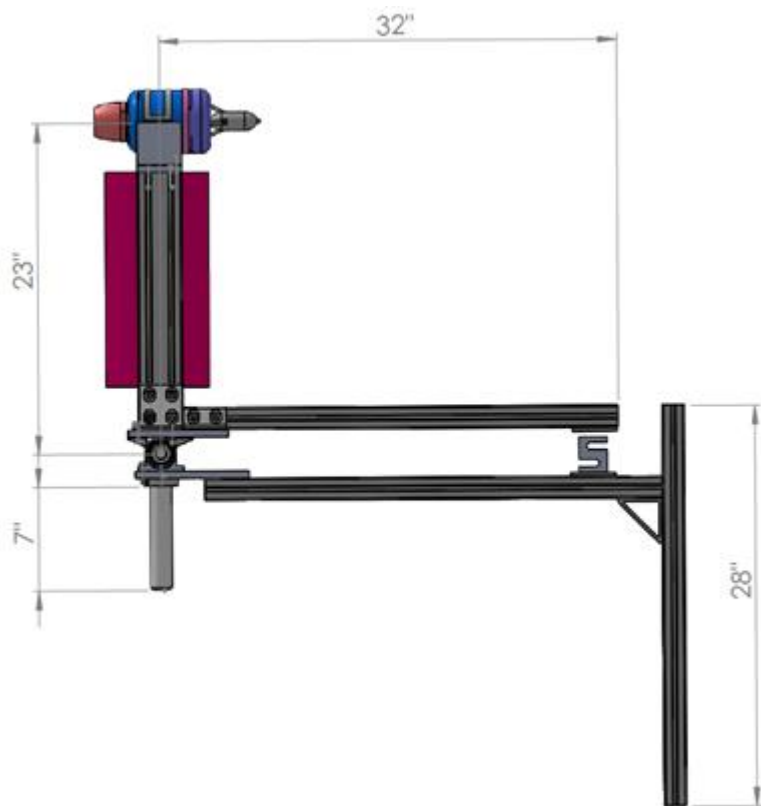


Figure 3.3 Profile and Dimensions of Final Thrust Stand Design

Figure 3.3 above shows that the load cell is bolted to a plate which is free to slide in the T-slotted framing. The distance from the pivot to the jet is 23", while from the pivot to load cell is 32" as shown. This allows the load cell force to be de-amplified by a factor of about 1.4 compared to the thrust force. Thus, maximum allowable jet force as limited by load cell is $1.4 \times 50\text{lbs} = 70\text{lbs}$.

Table 3.1 below shows at what force the remaining mechanical components would fail, based on the calculations in chapter 2. The maximum thrust produced by the JetCat p108x is 44lbs, so this load cell is sufficient for this project. However, for testing of larger jet engines in future projects, this jet stand can still be used but will require a load cell with a larger maximum capacity.

Table 3.1: Failure Modes

COMPONENT	MAXIMUM ALLOWABLE JET THRUST (LBS)
HORIZONTAL BEAM	490
VERTICAL BEAM	2880
BOLT GROUP 1	311
BOLT GROUP 2	525
BOLT GROUP 3	300
BOLT GROUP 4	640
LOAD CELL	70

Since the test apparatus blocks a portion of the test section, velocity variation relative to the upstream wind tunnel velocity must be considered. This velocity variation due to blockage was approximated using equation 3.1 below [9]

$$\frac{u_1}{V} = 0.62 * \frac{V_{model}}{V_{Test\ Section}} \quad (3.1)$$

$$\frac{u_1}{V} = \frac{270\text{in}^3}{(36\text{in})^2 \times (60\text{in})^2} = 0.0034 = 0.34\%$$

Where V_{model} includes the both JetCat, and portion of the mounting structure exposed in the wind tunnel for the most conservative estimate. A velocity variation of 0.34% is negligible and the effect of blockage can be ignored for the upcoming experiments.

Assembly and Manufacturing Procedures

For the finalized system design, a bill of materials was created to organize the potential sources and costs of the required parts, as shown below in Figure 3.XX.

Bill of Materials						
Component	Source	Part #	Qty	Cost \$	Status	
Adapter Materials						
Mounting Clamp**	JetCat USA		1	-	-	
Adapter plate	Midweststeelsupply		2	\$20.00	-	
Al Plate large 0.5 x 3ft x 6"	Midweststeelsupply		1	\$78.00	-	
Beams and Brackets						
Verical 8040 2ft	McMaster Carr	5537T111	1	\$35.56	-	
Verical 8040 3ft	McMaster Carr	5537T112	2	\$105.54	-	
Horizontal 40/40 3ft	McMaster Carr	5537T102	1	\$29.89	-	
Double Gusset Bracket	McMaster Carr	5537T6	2	\$28.00	-	
Single Gusset Bracket	McMaster Carr	5537T665	2	\$27.56	-	
Shaft						
1" Mounted bearing	McMaster Carr	5913K64	2	\$25.38	-	
1" Shaft x 12"	McMaster Carr	1346K37	1	\$25.42	-	
1" Shaft support	McMaster Carr	1865K6	2	\$50.62	-	
Base						
Base Plate 1/2" x32"x10"	Midweststeelsupply			\$61.16	-	
Mounting Plate						
Mounting plate 1/2"x10"x7"	Midweststeelsupply			\$20.00	-	
Additional Materials						
Connecting Bolts and Nuts	McMaster Carr			\$74.25	-	
Electrical Equipment	Various			\$550.00	-	
** = Provided By Dr. McCrink						Total (with Tax): \$1,196.43

Figure 3.4 Bill of Materials

The thrust stand was separated into various sections, and parts for each section were then listed, with potential sources and prices listed. Where possible, Part numbers was noted as well. A breakdown of the additional materials can be found in the appendix in Figure A.4. The electrical equipment budget assumed the team would need to purchase a new load cell, since the load cell provided by Dr. McCrink may not be sufficient to capture accurate and reliable data.

Assembly of the parts is straightforward, and most items are commercially available. Any custom parts that need to be manufactured can be fabricated using resources at the Center for Design and Manufacturing Excellence (CDME). The electrical system also requires minimal assembly.

Prototype Plan

Parts will be purchased from the sources found in the bill of materials (BOM) by submitting a purchase order such that they arrive before the start of the spring semester. The thrust stand and electrical system would be built and tested separately, and then integrated to construct the final testing system.

The initial test would be a static test that is conducted outside, and would serve to validate the thrust stand, data collection, and system identification system. Once the JetCat engine's static performance is well characterized, and testing system is validated, dynamic testing experiments can be conducted in a 3'x5' subsonic wind tunnel located at the Ohio State University Aerospace Research Center ("ARC"). The data to be collected from the experiments is represented in the figure below:

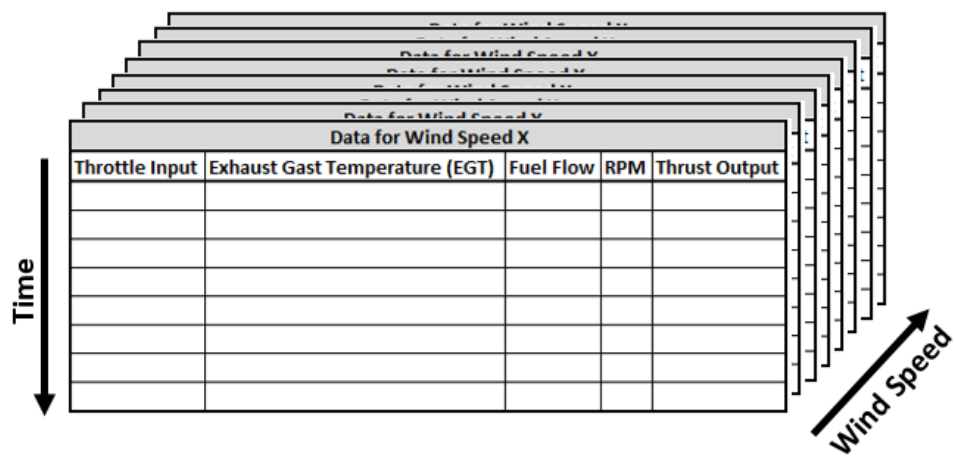


Figure 3.5 Experiment Testing Matrix

The exact discretization in windspeed and throttle inputs will be determined after initial tests are performed, as well as the number of trials conducted for each wind speed and throttle setting. The validation of the developed model requires an iterative approach to constantly improve model accuracy. An overview of the testing process is shown here:

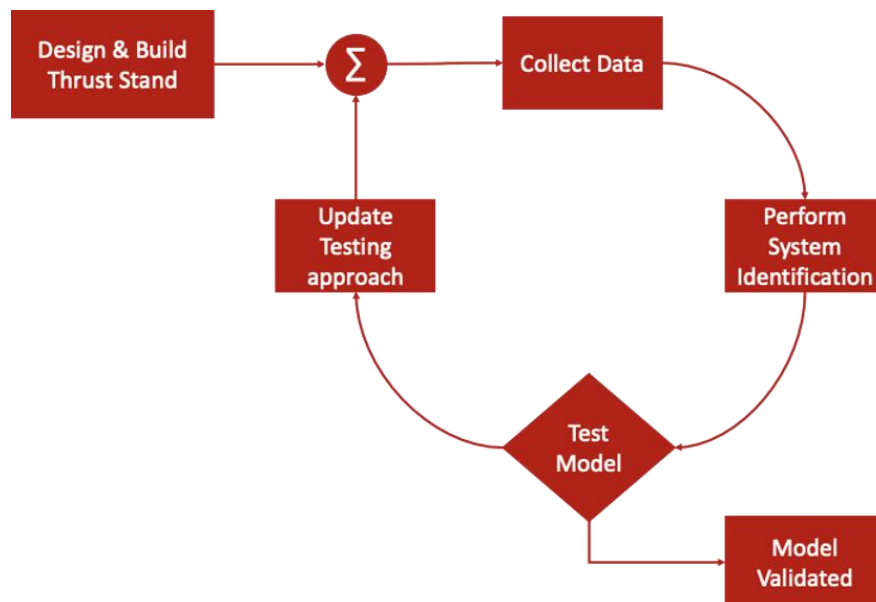


Figure 3.6 Test Process and Validation Plan

The thrust stand (with electrical system) is required to begin the testing and validation procedures. Once those systems are built, the team may collect data and test the modeling approach (for both static and dynamic scenarios). More specifically, the model would be validated by re-testing the system, and comparing recorded thrust to the estimated thrust provided by the model. Once error is within an acceptable range (dependent on throttle), the model would be considered validated.

Prototype Risk Assessment

While a plan is in place, every plan is susceptible to unpredictable mishaps and delays. To mitigate these potential delays, the process must have built in procedures clearly defined in the event of a postponement. Consequentially, risks need to be identified and strategically accounted for before they occur. Some of the potential risks for this project include delay in receiving parts, schedule conflicts for using the wind tunnel, and electrical/software troubleshooting.

To mitigate parts being delayed, the team will order parts before the start of winter break to maximize the time available to work. If the parts are delayed, the team will shift tasks in parallel to work on identifying key components with the ECU and troubleshooting the electrical and software setup. This would feed two birds with one scone as this a contingency plan for both delayed parts and troubleshooting. The team will be in contact with Dr. McCrink for the availability of the wind tunnel. If availability does become an issue, reservations will be made to have specific time for the team to conduct tests.

Chapter 4 – Final Design

Thrust Stand Development

Once all parts making up the test stand design had arrived, manufacturing the custom parts and stand itself began. Several pieces needed to be custom build, such as the engine adapter piece and base plates with bolt hole configurations. These were manufactured using a combination of end mills and CNCs to an acceptable tolerance level. Below in Figure 4.1 shows each of the different custom pieces build for the stand.

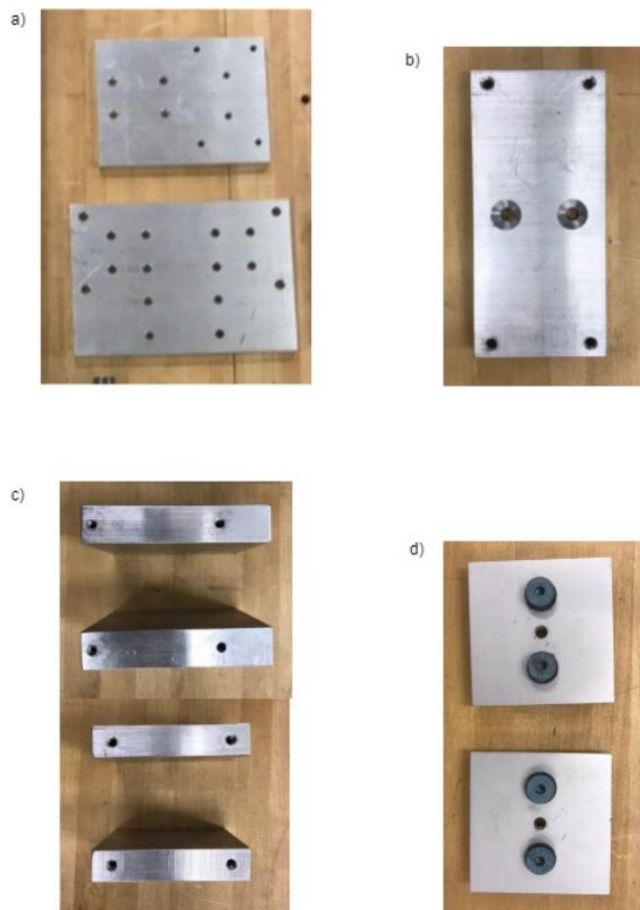


Figure 4.1: Custom built pieces for the jet stand with a) base plates, b) bottom engine adapter piece, c) side engine adapter pieces, both sides shown with threaded holes, and d) load cell slide plates.

Each piece, with exception to the load cell slide plates, were squared up to the drawing specification size, and either milled or drilled. Only the side engine adapter pieces required threads to bolt to the engine collar and bottom engine adapter piece. Drawings for each of these pieces can be seen in the Appendix, and are also located on the flash drives. Once these pieces were made and the 80/20 beams were cut to length, several holes needed to be drilled into the horizontal load cell beam at discrete locations. Below in Figure 4.2 shows these drilled holes.

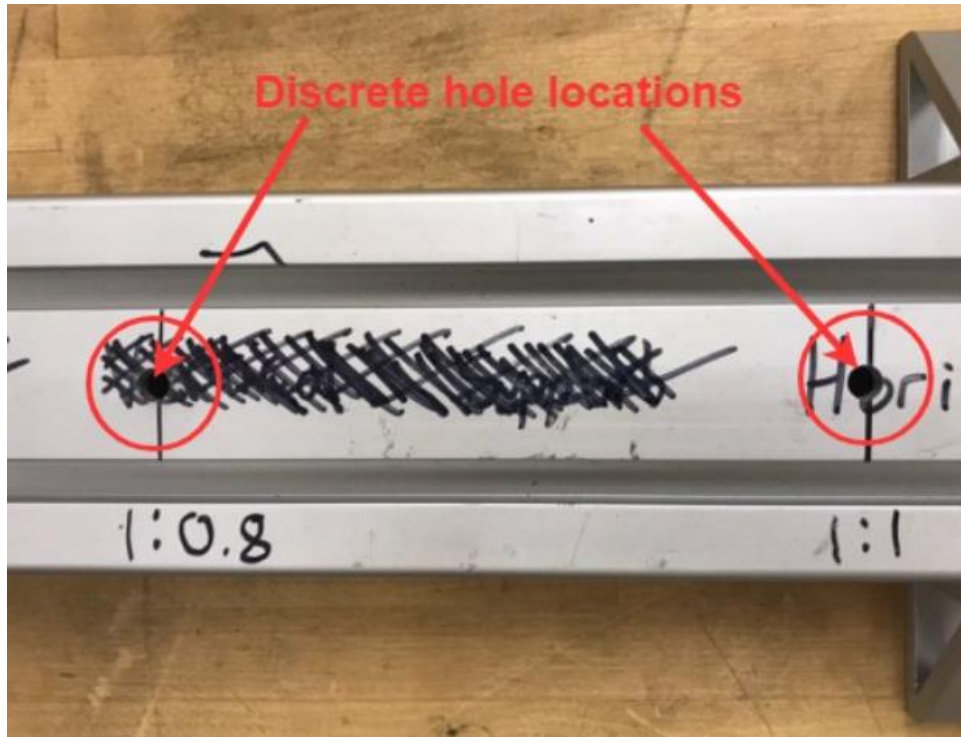


Figure 4.2: Beam hole locations for load cell placement.

These holes were drilled to allow a bolt through the beam and thread into the load cell. They were drilled at locations to give a force amplification of 1:1, and 1:0.8 thrust to load cell force. More holes can be drilled within the beam for a desired force amplification. Finally, the jet stand was able to be completely manufactured, and Figure 4.3 below shows the product.



Figure 4.3: Fabricated jet stand with load cell attached.

Electrical Hardware and Software Development

To collect the data needed for this project, an electrical system had to be designed and developed from the ground up by the team. As noted in the previous chapter, a variety of data had to be recorded, in addition to the load cell that is connected to the thrust stand. For the desired transfer functions, the team set out record the following:

- From external sources:
 - Thrust (from load cell)
 - From Electrical Controller Unit (ECU):
 - RPM
 - EGT (deg. C)
 - Throttle input (%)

At a high level, the system was designed with simplicity and flexibility in mind. For that reason, a single Arduino Mega was used as the hub to interact with all the sensors and relay the information back to a connected computer. Further, JetCat engines with a v10 ECU can return the required data via a serial request (detailed later). The final (user friendly) schematic of the system is shown in figure 4.4.

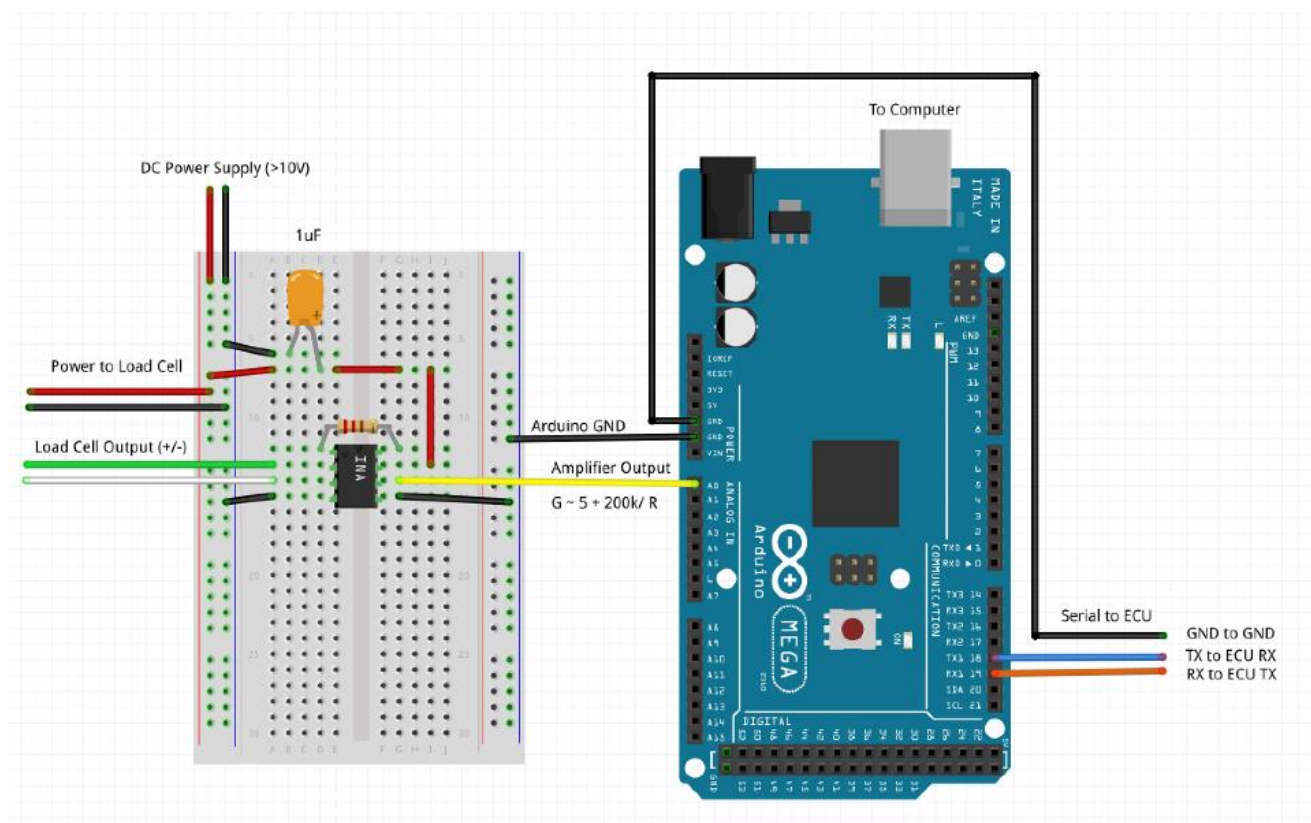


Figure 4.4 Schematic of Electrical Hardware

The load cell used (a LCCA-50) required a 10V DC power supply, and output $\pm 3 \text{ mV/V}$ (e.g., 30 mV for a 10V P/S at full compression). For the load cell power supply, a common DC bench power supply was used to provide 12.5 V. Provided that the Arduino cannot resolve data at a high enough resolution (can only resolve ~3-5mV increments), an amplifier was needed to increase the voltage output of the load cell. As such, an instrumentation amplifier (INA122, DIP package) was used to amplify the signal within a range able to be read well by the Arduino's analog input (0 to 5 volts). The INA122 was connected based on the schematics found in the data sheet, and the resistor was chosen based on the desired gain for our signal. Once connected as shown, the load cell output could be read using the `analogRead()` command. To be able to determine the thrust (in lbs., N, etc.), the system needed to be calibrated, details on which will be described in the next section.

The JetCat ECU records a variety of parameters as the engine is running, which can be accessed via serial command. To connect to the ECU, the team connected the Arduino TX1/GND/RX1 ports to the ECU RX/GND/TX ports (respectively), using a provided pre-soldered LED I/O board. Note that this board still allowed for the nominal ground support unit (GSU) connection. The Arduino `Serial#.write()` and `Serial#.read()` commands were then used to send and receive information to and from the ECU.

Once connected and in working order, the system was then updated (via software commands) to operate at 38,400 baud (instead of the default 9600), in order to allow for higher sampling frequencies. This requirement was driven by system, as higher sampling frequencies are needed to properly capture higher frequency modes.

A script was written in the Arduino language that continuously recorded the following parameters, at about 16.67Hz:

- Load Cell
- RPM
- EGT
- Pump Voltage
- Turbine State
- Throttle

The data was recorded by sending information to the Serial monitor, and copying the monitor window data to a text file at the end of each trial. For more details on the script (and all scripts used for the electrical system), please refer to the files found on the accompanying flash drive(s).

After test data was recorded, the data needed to be processed to ensure readings were accurate and there were no missing values. Provided the high sampling rate and long run time of trials, the length of recorded data grew beyond human-correction levels. Thus, a Python script was created to “clean” the data.

The Python program went through each line of the text file (recorded data), and continuously added to a running list of each parameter (e.g., creating a list of load cell readings, and a separate list for

RPM, etc.). For times when a value was skipped or there was an extreme outlier, the previous value was substituted. Other edge cases were considered and treated as well (i.e., missing trailing zeros). Such errors in the data were on the order of 0.01% of the total amount of data recorded (generally less). Once the data was cleaned, the file recorded the information to a CSV file that could easily be opened in Excel or MATLAB.

Load Cell Calibration

Load cell calibration was done by applying a horizontal force to the jet stand at the location where the jet is normally mounted. The pulley setup provided by Jet Master Jake is shown in the appendix. The applied force was varied from 0-45 lbs, producing the calibration curve shown in figure 4.5.

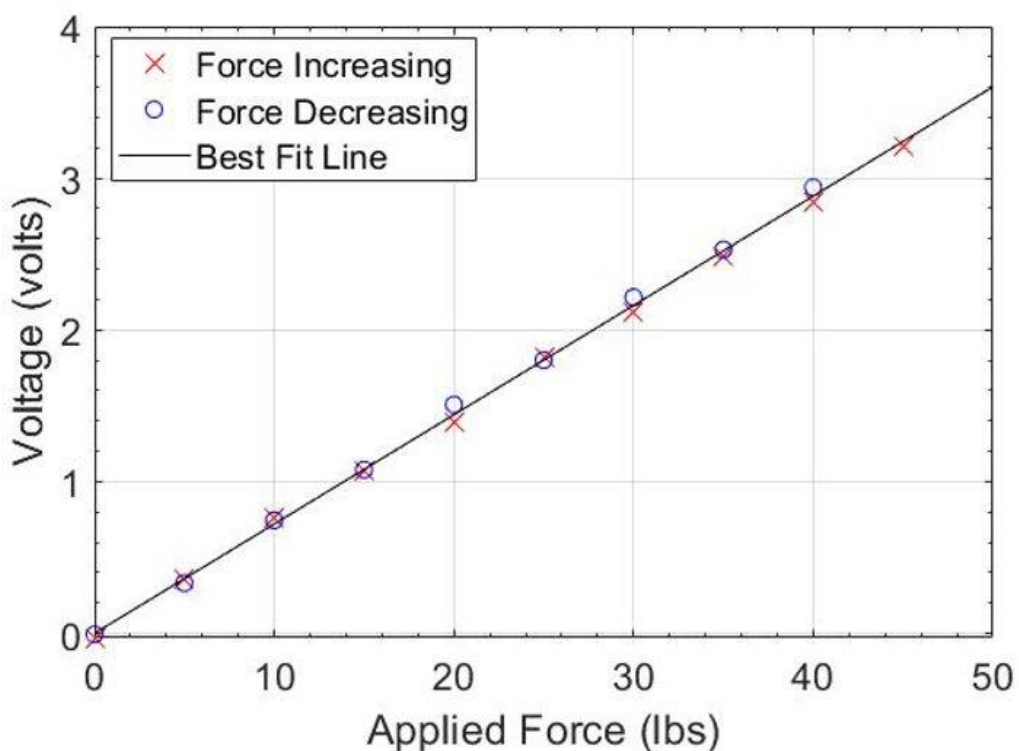


Figure 4.5: Jet stand calibration, after being zeroed. **Equation: $F = 13.862V \pm 0.017$ lbs**

The uncertainty in the measurements was taken as the average deviation of each point from the best fit line. This is roughly 0.033% full scale, which is in the ballpark of the uncertainty provided by the manufacturer (see reference [6]). Other sources of error in the calibration include the possibility of the cable pulling at a slight angle, and the table to which the stand is mounted moving slightly during the calibration.

Results Summary

After successfully building the thrust stand as described in the previous sections, experimentation was conducted with the JetCat P-180 engine in the Rocket Pit of Bolz Hall to collect data regarding both its turbine speed and thrust transience response to throttle inputs. Once the engine's response data was collected and filtered, System Identification was performed through MATLAB's System Identification Tool Box as to calculate a transfer function that fit the experimental data well. In this section, the results of performing System Identification on the experimental data are presented.

The first test showed oscillations in load cell reading with amplitudes as large as the actual force shown in figure 4.6. It is suspected that the majority of the vibration is in the tall vertical beam which the jet is mounted to, as well as the table the entire stand is mounted to, which is fairly unstable. Addition of a 45 degree beam shown in figure 4.6 significantly reduced the oscillations. The vibrations could still be reduced further with a more rigid vertical beam, which should be done as a part of future work.

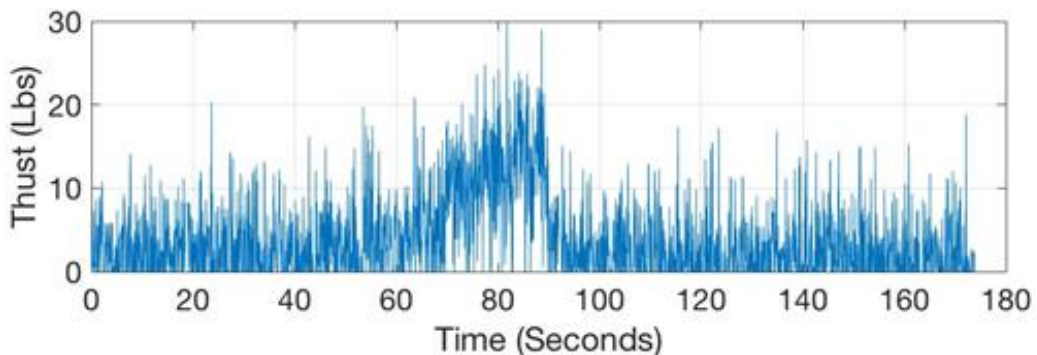


Figure 4.6: Load cell readings without 45 degree beam



Figure 4.7 Thrust stand with 45 degree beam installed

The reduction of oscillations can be seen in figure 4.8a. The remaining high-frequency noise in the data was attenuated using a low pass filter with a 0.25 Hz cut off, and a 20 sample moving average, shown in figure 4.9b. Note that although the vibration is removed enough to roughly see the steady state thrust values for each step, the remaining noise will likely skew the transfer functions slightly.

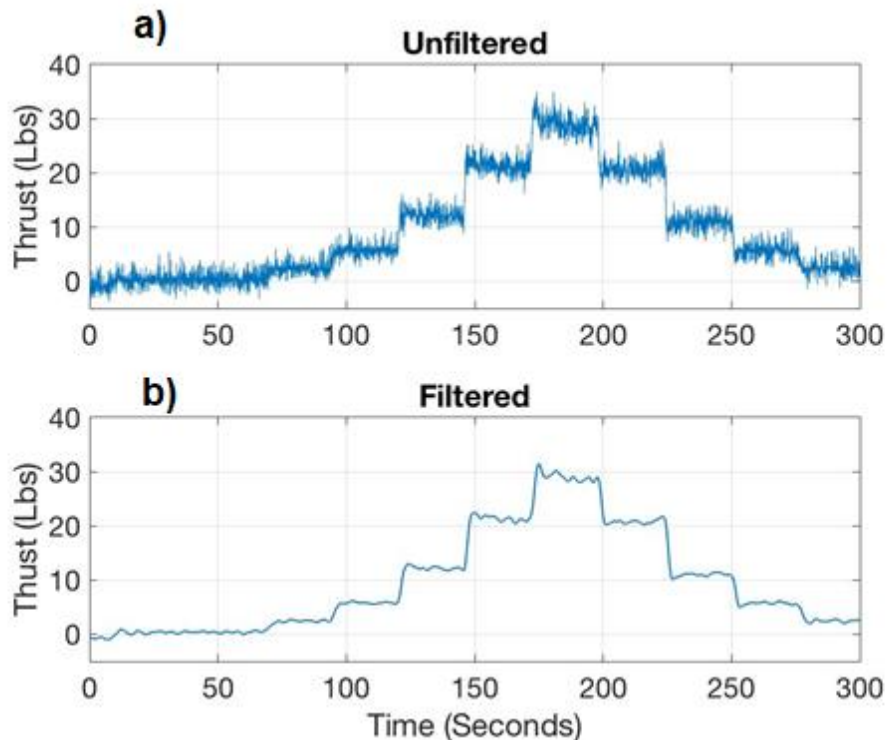


Figure 4.8: Load cell readings with 45 degree beam a) raw data b) filtered data

Once experimental data collection for the P-180 engine was completed, System Identification was performed on each set of step response data in order to compute transfer functions relating both turbine speed and thrust to a controllable input variable. For each set of step response data, 45 different general forms of transfer functions were iteratively fitted to the experimental RPM and thrust data. Specifically, 1st ordered, 2nd ordered, and 3rd ordered transfer functions were utilized in the System Identification process. Although higher ordered systems could have been investigated, it was decided to not exceed a 3rd ordered transfer function as physical insight to the engine's behavior begins to degrade as the transfer function's order increased. In addition to varying the transfer functions' number of poles, the number of zeros was also varied. Furthermore, it was determined to investigate transfer functions that displayed underdamped behavior as overshoots were visually detected in both the RPM and thrust data. Lastly, general transfer function forms equipped with a time-delay term were also investigated. After deciding which general transfer functions to fit the experimental data via System Identification, specific transfer functions with numerical values were calculated for both engine speed and thrust.

The initial transfer functions derived from the experimental data related throttle setting to the engine's turbine speed and thrust. Although throttle setting appeared to be the obvious choice for the transfer functions' control variable, the resulting throttle-RPM and throttle-thrust transfer functions did not meet our expectations or requirements. Despite the fact that the resulting analytical transfer functions fit the experimental well, the fitted coefficients varied wildly between consecutive step-responses with no apparent trend. For example, the natural frequencies computed for a 2nd ordered throttle-RPM transfer function varied several orders of magnitude for consecutive throttle steps even though the average fit was approximately 90%. It is believed that neither the turbine speed nor thrust is linearly related to throttle's position, voiding the assumption that linear transfer functions can relate throttle setting to the engine's performance. Since the fitting coefficients for both the throttle-RPM and throttle-thrust transfer functions were radically different between step inputs and did not provide insight into the engine's true nature, it was ultimately decided to abandon throttle-based transfer functions.

After concluding that throttle-based transfer functions did not accurately describe the Jetcat P-180's response to step inputs, it was decided to base future transfer functions off of a different control variable. Specifically, System Identification was performed on the experimental data for transfer functions that relate the ECU's commanded RPM to both the engine's measured turbine speed and thrust. As done with the previous transfer functions, 45 different general forms were fitted to the experimental data by varying the number of poles, number of zeros, degree of damping, and time delay for the commanded RPM-actual RPM and commanded RPM-thrust transfer functions. After performing System Identification on these general transfer functions where commanded RPM was the control variable, it was concluded that the resulting mathematical models more accurately described the engine's true nature as the analytical results fit the experimental data well and the fitting coefficient did not vary as dramatically. In the following paragraphs, specific results for the commanded RPM-actual RPM and commanded RPM-thrust transfer functions are presented.

After performing System Identification for all 45 possible transfer functions relating Commanded RPM to Actual RPM, it was concluded that an underdamped, second-ordered system with one zero and no time delay best described the transient behavior of the engine's RPM spool-up. The general form of this Commanded RPM-Measured RPM transfer function is presented below, where K_p is the transfer function's gain, ω_n is the engine's RPM natural frequency, ξ is the damping ratio, and τ_z corresponds to the transfer function's zero.

$$\frac{RPM(s)}{RPM_{Command}(s)} = \frac{K_p(1 + \tau_z s)}{\omega_n^2 s^2 + 2\xi\omega_n s + 1}$$

Additionally, the average numerical values and standard deviation corresponding to each variable in the above transfer function are presented below in Table 4.X. Although the transfer function's general form remains valid for both step-up and step-down commands, it should be noted that the numerical values of the transfer function change depending on the direction of commanded RPM. While the transfer function's natural frequency remains nearly constant at 0.55 rad/sec for both step-up and step-down commands, the step-up damping ratio of 0.76 is larger than the damping ratio of 0.58 corresponding to the step-down transfer function. Additionally, it should be noted that the transfer function's zero location is not reliable as the standard deviation of its position is of the same magnitude of its average position. Although the zero's location varies between throttle steps, the overall fit of the two Commanded RPM-Measured RPM is approximately 85%. In addition to Table 4.1 below, Figures 4.9 and 4.10 visualize the experimental and analytical RPM results to a step command. Suggestions on how to improve the Commanded RPM-Measured RPM transfer function are presented in *Future Work*.

Table 4.1: Average Numerical Values for RPM Transfer Function

Model	K_p	ω_n	ξ	τ_z	Avg. Fit
Commanded RPM-RPM (Up)	1.0 [+/-0.001]	0.566 [+/-0.074]	0.761 [+/-0.012]	-0.989 [+/-0.840]	85.98% [+/-3.19]
Commanded RPM-RPM (Down)	1.0 [+/-0.0003]	0.554 [+/-0.039]	0.575 [+/-0.067]	1.393 [+/-2.103]	85.18% [+/-3.84]

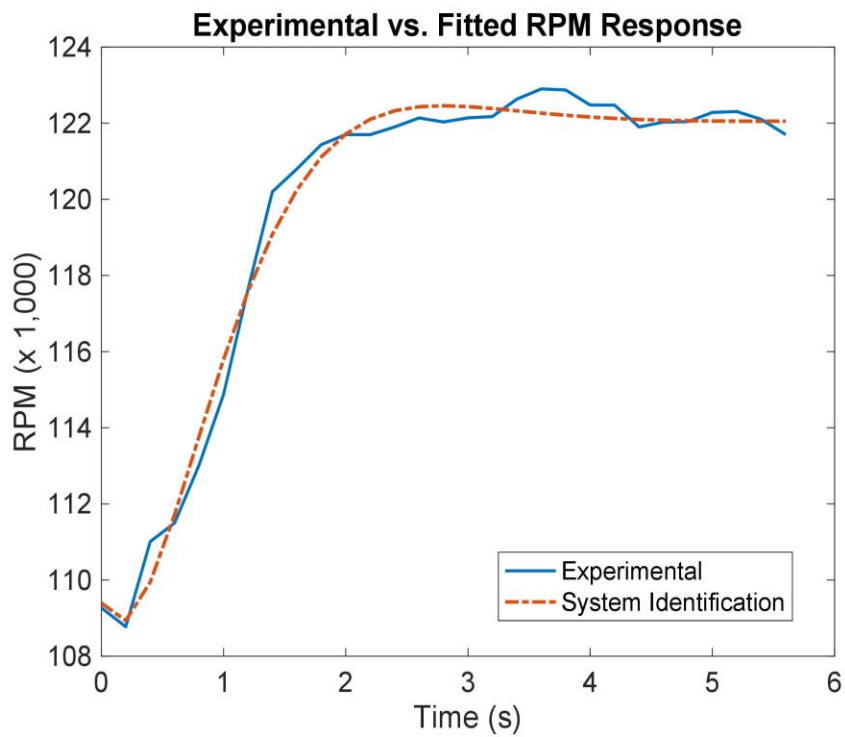


Figure 4.9: Comparison of Experimental Data and Theoretical Fit on a Dropping RPM Interval

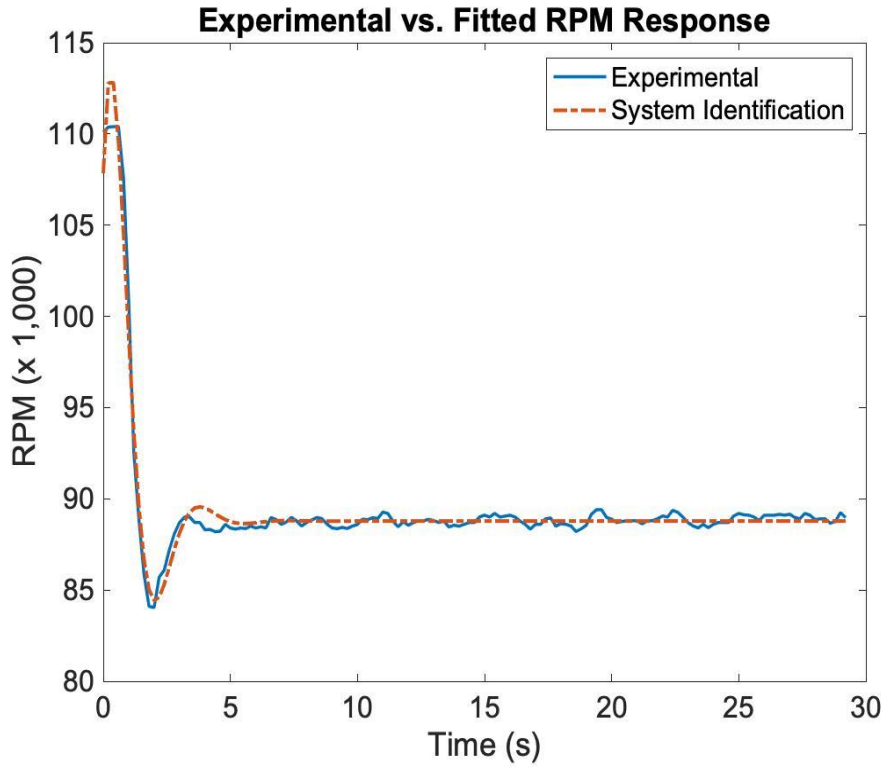


Figure 4.10: Comparison of Experimental Data and Theoretical Fit on a Rising RPM Interval

After computing a Commanded RPM-Measured RPM transfer function, work continued by determining a transfer function relating a commanded RPM to thrust output. Unlike the Commanded RPM-Measured RPM transfer function, the best Commanded RPM-thrust transfer function was determined to be an underdamped third ordered system with one zero and no time delay. This form of transfer function is presented below, where K_p , ω_n , ξ , τ_z are defined above and τ_p corresponds to the third pole.

$$\frac{Thrust(s)}{RPM_{Command}(s)} = \frac{K_p(1 + \tau_z s)}{(\omega_n^2 s^2 + 2\xi\omega_n s + 1)(\tau_p s + 1)}$$

As with the Commanded RPM-Measured RPM transfer function previously described, the Commanded RPM-Thrust transfer function had different numerical coefficients dependent upon the direction of the commanded signal. Although the model's natural frequency did not drastically vary from an average value of 0.93 rad/sec, the damping ratio displayed the same behavior as with the Commanded RPM-Measured RPM transfer function. Specifically, step-up responses had a larger damping ratio of 0.69 than the damping ratio of 0.47 associated with step-down responses. This change in damping ratio is visualized by the more dramatic overshoots in step-down thrust response, as shown in Figures 4.11 and 4.12. Furthermore, both the results for the zero, τ_z , and third

pole, τ_p , of the Commanded RPM-Thrust transfer function are not reliable as the standard deviation associated with these characteristics are of the same magnitude as the average positions. Additional work should be done in the future to develop a better Commanded RPM-Thrust transfer function.

Table 4.2: Average Numerical Values for Thrust Transfer Function

Model	K_p	ω_n	ξ	τ_z	τ_p	Avg. Fit
Commanded RPM-Thrust (Up)	0.000186 [+/-0.00006]	0.890 [+/-0.142]	0.687 [+/-0.287]	-0.678 [+/-0.415]	0.412 [+/-0.249]	83.2% [+/-12.2]
Commanded RPM-Thrust (Down)	0.0001225 [+/-0.00005]	0.969 [+/-0.163]	0.473 [+/-0.212]	-0.594 [+/-2.355]	0.537 [+/-0.554]	83.65% [+/-3.82]

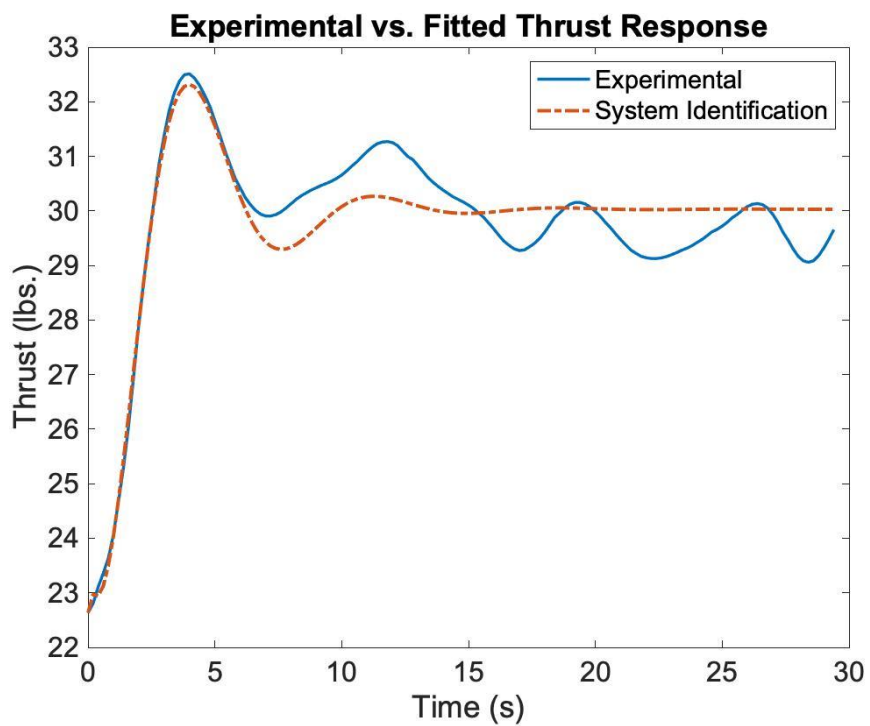


Figure 4.11: Comparison of Experimental Data and Theoretical Fit on a Rising Thrust Interval

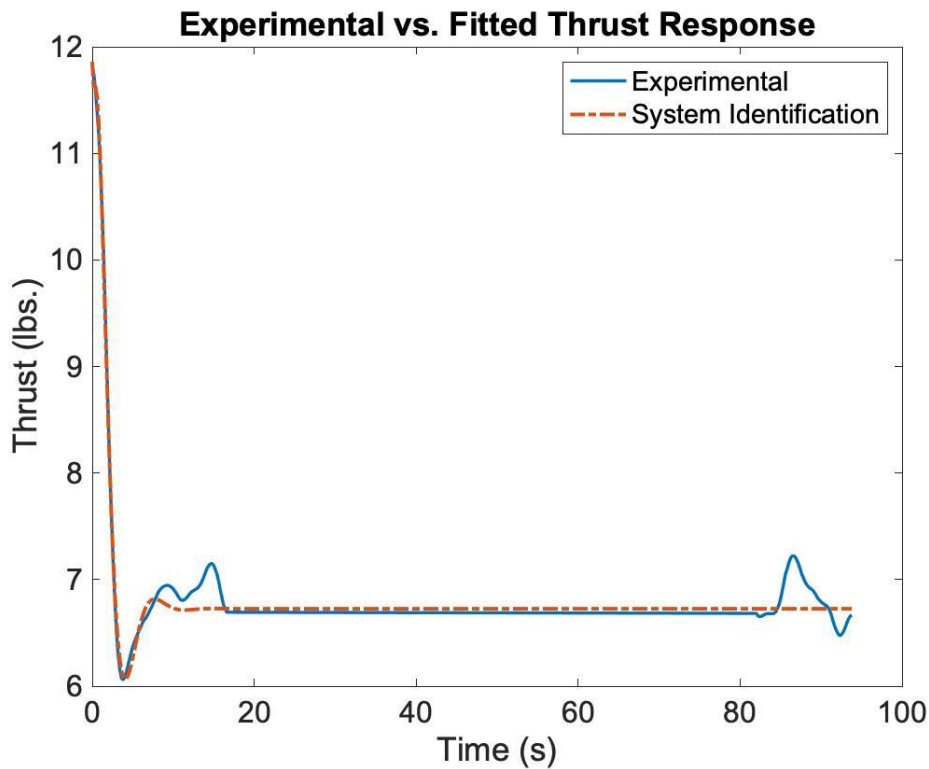


Figure 4.12: Comparison of Experimental Data and Theoretical Fit on a Dropping Thrust Interval

In addition to analyzing engine data collected during this year's capstone project, flight test data recorded in the summer of 2017 was used to compare the previously discussed results to an unrelated data set. Only the Commanded RPM-Measured RPM transfer function's results were compared to flight test data as the thrust response was not recorded in Dr. McCrink's experiment. As shown below in Table 4.3, the numerical values associated with the Commanded RPM-Measured RPM transfer function derived from flight test data did not match the values listed in Table 4.1. Although the exact numerical coefficients based off of flight test data did not match the thrust stand's results, the same general trends regarding natural frequency and damping ratio persisted. Specifically, the natural frequency of the RPM's transfer function remained nearly constant between step-up and step-down commands. Additionally, the damping ratio was higher for increasing RPM commands than for decreasing RPM commands. A possible explanation for the numerical differences between data sets is that the flight test information included side-effects associated with the airframe, namely air-intake influences and non-zero freestream velocities. Although the numerical values associated with the transfer functions differ between data sets, the general form of an underdamped second-ordered system with one zero appears to predict the RPM transience well.

Table 4.3: Average Numerical Values for RPM Transfer Function from Flight Test Data

Model	K_p	ω_n	ξ	τ_z	Avg. Fit
Commanded RPM-RPM (Up) [Flight Test Data]	1.0 [+/-0.0007]	1.443 [+/-0.233]	0.769 [+/-0.074]	-0.898 [+/-0.237]	95.01% [+/-1.74]
Commanded RPM-RPM (Down) [Flight Test Data]	1.0 [+/-0.0004]	1.483 [+/-0.187]	0.633 [+/-0.042]	-0.825 [+/-0.112]	94.22% [+/-2.72]

Budget Breakdown

Currently, none of the funds have been used and the entire \$3,500 is available. During the end of the fall and spring semester, we anticipate spending approximately \$1,275. The breakdown is as follows:

Table 4.# Budget Breakdown

Item	Projected Cost (\$)
<i>Thrust Stand Material</i>	650
<i>Electrical Equipment</i>	550
<i>Fuel</i>	75
Total:	\$1,275

Table 4.# Budget Breakdown

Item	Projected Cost (\$)
<i>Thrust Stand Material</i>	650
<i>Electrical Equipment</i>	550
<i>Fuel</i>	75
Total:	\$1,275

The electrical equipment refers to various electrical components and sensors (e.g., strain gage), and fuel is needed to power the engine during testing.

Conclusion/Future Work

As the initial goal of the project was to obtain transfer functions for a variety of wind conditions, future teams should look to implement the stand within the wind tunnel. However, there are some foreseen issues with this. The addition of the 45 degree beam could potentially obstruct flow in front of the engine, especially if a larger beam is added. The larger problem would be sealing the bottom of the wind tunnel, as now the stand has two points of penetration into the tunnel. These parts of the stand itself cannot touch the wind tunnel, or valuable load cell data will be altered. But the tunnel must be sealed enough around these points to not significantly change the pressure during wind tunnel operation. One solution to this problem would be to either redesign the baseplates or simply flip them 180 degrees, and have the load cell in tension. Other design modifications might be needed as obstructions were noted to be behind the beta table under the wind tunnel.

Upon completion of the project, it was uncovered that the engine was simply controlled by dumping more fuel into the exhaust as throttle was increased. This fuel corresponds to an integral pump voltage, which can be backed out from the ECU. This results in the difference in the step-up and step-down transfer. Performing more experiments and capturing this data may prove to be useful for creating an accurate engine model.

The team's models assumed a step function was commanded to the engine, when in reality it was an aggressive ramp estimated using the RC controller. Inputting an exact step for throttle control in many different discrete steps could yield better system identification results. This can be done using the Arduino and sending a commanded RPM to the ECU.

References

- [1]: Chapman, J., Lavelle, T., & Litt, J. (2016). Practical Techniques for Modeling Gas Turbine Engine Performance. Retrieved October 9, 2018.
- [2]: Fozo, L., Andoga, R., & Kovacs, R. (2016). Thermodynamic Cycle Computation of a Micro Turbojet Engine. *17th IEEE International Symposium on Computational Intelligence and Informatics*. Retrieved October 9, 2018.
- [3]: Gao, J., & Huang, Y. (2011). Modeling and Simulation of an Aero Turbojet Engine with GasTurb. Retrieved October 9, 2018.
- [4]: Kiyak, E., Yasa, T., & Yazar, I. (2017). Simulation-Based Steady-State Aero-Thermal Model for Small-Scale Turboprop Engine. *Aircraft Engineering and Aerospace Technology: An International Journal*. Retrieved October 9, 2018.
- [5]: Matsson, J. (2004). Laboratory Experience with a Model Jet Turbine. *American Society for Engineering Education Annual Conference & Exposition*. Retrieved October 9, 2018.
- [6] Omega LCCA datasheet: <https://assets.omega.com/pdf/test-and-measurement-equipment/load-and-force/load-cells/LCCA.pdf>
- [7]: Ruina, A. (2013, November 19). Intermediate Dynamics and Vibrations. Retrieved November 1, 2018, from <http://ruina.tam.cornell.edu/Courses/ME4730 Fall 2013/>
- [8]: Schewe, G. (2013). Reynolds-number-effects in flow around a rectangular cylinder with aspect ratio 1:5. *Journal of Fluids and Structures*, 39, 15-26. doi:10.1016/j.jfluidstructs.2013.02.013
- [9]: Yang, J., & Zhu, J. (2015). Dynamic Modeling of a Small Scale Turbojet Engine. *European Control Conference*. Retrieved October 9, 2018.

Appendix

Original Problem Statement

 THE OHIO STATE UNIVERSITY
COLLEGE OF ENGINEERING

JETCat

 THE OHIO STATE UNIVERSITY
COLLEGE OF ENGINEERING

Department of Engineering Education
Multidisciplinary Design Capstone

OSU Jet Cat

Dr. McCrink has set the world record for longest UAV flight over an out-and-back course. The vehicle flew autonomously with sustained speeds around 147 mph!

McCrink wants to go faster, further, most efficient.

This project is a continuation from last year's but will potentially be applied his future UAV in current development.





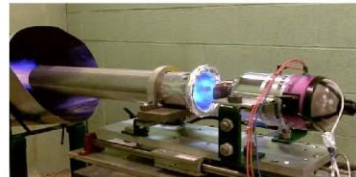
2

 THE OHIO STATE UNIVERSITY
COLLEGE OF ENGINEERING

Department of Engineering Education
Multidisciplinary Design Capstone

Objective:

- Conduct performance calibrations of a Jet Cat engine via ground and wind tunnel testing
- Utilize an in-house built thrust stand to calibrate the engine's static performance
- Mount thrust stand in the subsonic wind tunnel at the ARC
- Look at inlet design



3

Team Charter

The Ohio State University

Team Charter

Jetcat P-180 Capstone Group:

Ross Heidersbach

Isaac Khan

Mark Luke

Tommy Malkus

Hamil Shah

Engr 5901.01

Bob Rhoads and Jake Allenstein

09/07/2018

Introduction

The purpose of the following team charter is to provide a brief context to the Jetcat capstone project as well as to identify the expected deliverables required at the culmination of the capstone project. Additionally, team roles are listed and described, which are then cross-referenced with personal skill-sets in order to assign individuals to specific lead positions. Team members' expected behaviors are then explicitly stated followed by a list of corresponding consequences and procedures for conflict resolution. Lastly, an approximate schedule of events is presented to guide the development and verification of a performance-based dynamics model of a Jetcat P-180 turbojet engine.

Context

This capstone group is tasked with creating an accurate performance-based plant model of a Jetcat P-180 turbojet engine, which is regularly utilized in high-performance radio-controlled (R/C) aircraft and Unmanned Aerial Vehicles (UAV). Specifically, engine parameters that will be investigated will include, but are not limited to, thrust values, fuel-flow measurements, and exhaust gas temperatures (EGT). The results of this capstone will be utilized at The Ohio State University's Aerospace Research Center for future high-speed UAV research conducted by Dr. McCrink. Specifically, the plant-model of the P-180 turbojet will be utilized for predicting jet engine performance in real-time as such information is required for autonomous auto-pilots and Stability Augmentation Systems (SAS). With the addition of an accurate engine plant model, autonomous flight controllers will be able to operate UAVs with an increased degree of efficiency and safety.

Mission and Objective

As described above, an accurate engine plant model is necessary for safe and efficient autonomous control of UAVs. The first objective of this capstone project is to complete a literature review of existing academic work regarding turbojet engines in general as well as Jetcat engines specifically. In this phase, team members should research what engine parameters are important for plant modeling as well as look for pre-existing thermodynamics relationships that equate engine inputs to performance outputs. After completing a thorough literature review, a theoretical plant model of the Jetcat P-180 is to be derived that predicts pertinent performance values for a given set of inputs. The next stage of the project is to design and build a test stand that can secure the turbojet engine and measure important parameters, such as thrust and fuel flow. Following the construction of the test stand, experimental performance data will be collected by operating the Jetcat engine at different environmental conditions. This experimental data will then be utilized to verify and further fine-tune the theoretical plant model derived earlier in the year.

Composition and Roles

The following roles will be fulfilled by the corresponding individuals:

Project Leader - Isaac Khan

- Responsibilities of the Project Lead include making sure the overall project follows the timeline, managing expenditures, and organizing team meetings.

Documentation Coordinator - Ross Heidersbach

- Responsibilities of the Documentation Coordinator include collecting and organizing all research material into one central database. Additionally, this role is responsible for compiling, formatting, and proofreading the PDR and CDR documents.

Fabrication Lead – Tommy Markus

- Responsibilities of the Fabrication Lead include overseeing the full design process of the test stand. This includes the design and fabrication of custom parts as well as the selection of off-the-shelf parts.

Hardware/Software Lead - Hamil Shah

- Responsibilities of the Hardware/Software Lead include implementing sensors and other electrical hardware. Additionally, this individual will work with the Experimental Lead to ensure that the electrical systems will support experimental data collection.

Safety Lead - Ross Heidersbach

- Responsibilities of the Safety Lead include ensuring that experimental tests are conducted in a safe manner. Specifically, this includes that safety equipment (i.e. fire extinguishers) is nearby during testing, that the engine does not exceed performance limitations (i.e. turbine RPM, EGT), and that team members conduct themselves in a safe manner.

Experimental Lead - Mark Luke

- The Experimental Lead will work in tandem with the Hardware/Software Lead with hardware selection for the experimental setup. Additionally, this individual will set up the test stand and mount hardware appropriately. Lastly, the Experimental Lead is responsible for confirming that the data collection process is accurate and appropriate for modeling needs.

Record Keeper - Isaac Khan

- Responsibilities of the Record Keeper include documenting information that was discussed in meetings and project work time. Photo documentation falls under this role. The Record Keeper and the Documentation Coordinator will work hand in hand to ensure all info is stored and readily available.

These roles were assigned to the corresponding individuals because these team members had an appropriate set of skills, as described below:

Ross Heidersbach

- Familiar with radio control aircraft and UAVs. Experience with micro turbojets. Novice at system identification and modeling, specifically via MATLAB/SIMULINK. Experience with experimental set-ups. Familiar with Arduino, Labview, MATLAB, SIMULINK, Solidworks, and XLFR-5

Tommy Malkus

- CAD design, basic manufacturing skills (machining, hole making, 3D printing). Computational Fluid Dynamics Modeling. Basic programming in C++ and MATLAB.

Isaac Khan

- Project organization and technical communication, LabView Certified, Robotics Experience, SolidWorks, Basic programming in C++ and Matlab.

Hamil Shah

- Electrical circuits, programming, and aircraft / spacecraft system modeling. Key programming abilities include MATLAB and Python. Circuit experience includes electrical lab courses, as well as setting up and calibrating sensors (IMUs, temperature, sun, etc.). Modeling work includes spacecraft trajectories and flying radar imaging performance. Novice with respect to actual engine modeling and certain concepts in thermodynamics and propulsion.

Mark Luke

- CAD design (SolidWorks), programming within MATLAB, basic C++, basic LabView, and Simulink. Course experience with measurements and analysis, and modelling of systems. Basic machining/fabrication skills.

Authority, Empowerment, Commitment:

It is expected that every member attend class, unless otherwise specified, or prior notice has been given. Verbal notice will be given for the first offense. After the second offense of a no-show, the team will see if there is any problem with meeting times or schedule conflicts that can be avoided. After the third offense, Jake Allenstein and Bob Rhoads will be involved to see if there is anything that can be done to fix the issue.

Individuals on the team can buy any equipment necessary for the project that is less than 5% of the remaining budget without majority team approval. Anything above, must require a team meeting before purchasing. Access to the Aerospace Research Center will be limited to normal business hours, unless otherwise approved by Dr. McCrink.

Weekly Meeting Operations:

Meetings will begin bi-weekly with Dr. McCrink on September 6 at 9:30am at the Aerospace Research Center (ARC, 2300 W Case Rd). The meeting time is tentatively set for the same time every two weeks after, which will be confirmed within a week of the next meeting. The Record Keeper and the Document Coordinator are responsible for noting and collecting all decisions, ideas, and up-coming tasks discussed during the bi-weekly meetings.

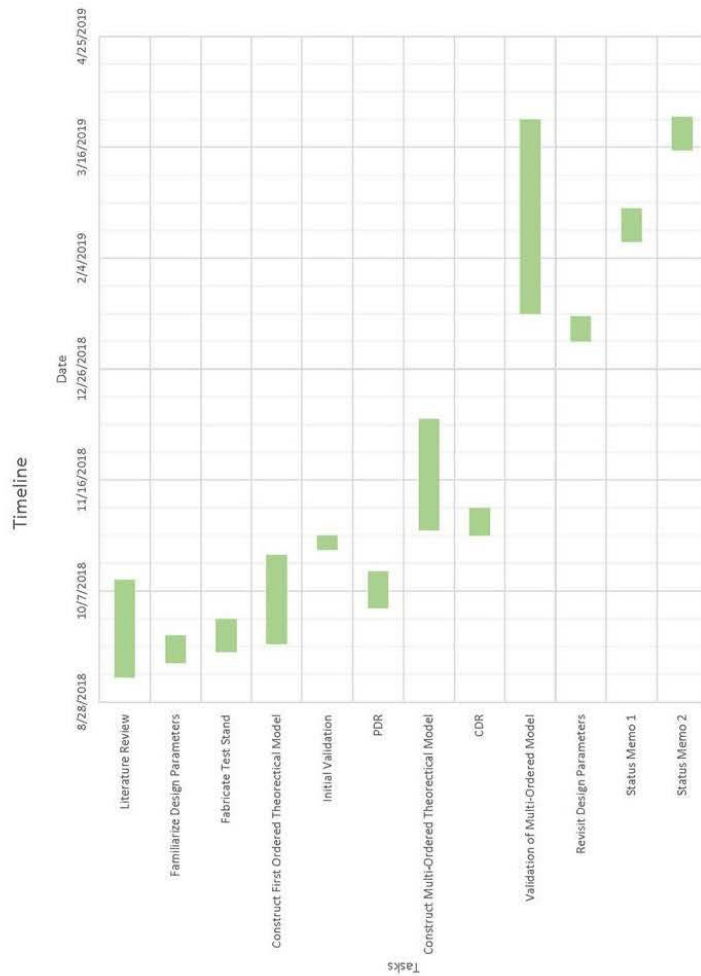
Conflict Resolution:

Lack of Personal Responsibility: If it is deemed that a member of the team is lacking in responsibility, the team will come together and detail the lack of responsibility as a first warning. If this problem continues, the team will come back together and reiterate the problem to the member and issue a second warning to him. If the problem persists after these attempts, Bob Rhoads and Jake Allenstein will be brought in to help address the issue. Clear communication is key. If there is an emergency, it is the member's responsibility to communicate this to the team at least 24 hours before, or as soon as possible.

Interpersonal Quarrels: If a member of the team feels they aren't being treated right, they should confront the specific member or team with the issue. If the conflict still exists after it is addressed, Bob Rhoads and Jake Allenstein will be brought in to help with the issue.

Technical Disagreements: A meeting will be held where each opposing argument will be made. If there is no agreement on which solution is correct, the arguments will be made to Dr. McCrink where his decision on technical issues will be final.

Approximate Schedule of Events:



Signatures:

Signature: Hamil Shah

Signature: Mark Luke

Signature: Isaac Khan

Signature: Tommy Markus

Signature: Ross Heidersbach

Problem Definition Presentation

THE OHIO STATE UNIVERSITY
COLLEGE OF ENGINEERING

OSU - Jetcat Problem Definition

Ross Heidersbach, Isaac Khan, Mark Luke, Tommy Malkus, Hamil Shah
ENGR 5901.01

Introduction

Team Introduction:

- Isaac Khan – Engineering Physics
- Ross Heidersbach – Mechanical Engineering
- Mark Luke – Mechanical Engineering
- Tommy Malkus – Engineering Physics
- Hamil Shah – Electrical and Computer Engineering

2

Background

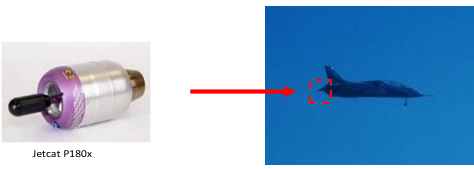
- For over the past 4 years, Dr. McCrink and other faculty members at the Aerospace Research Center (ARC) have focused on advancing Unmanned Aerial Vehicle(UAV) technology
- Specifically, Dr. McCrink researches and develops control laws utilized in autonomous UAVs



Image Source: Aerospace Research Center
Presenter: Ross H. 3

Background

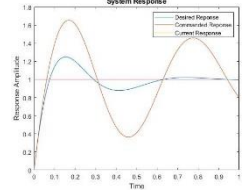
- Last September, two world records were set using Dr. McCrink's turbine powered UAV, known as the Avanti
- The Avanti flies at over 200 mph and has a take-off weight of 70lbs
- This aircraft is powered by a Jetcat P180x, a Micro-Turbojet engine which produces a maximum of 40lbs of thrust



Jetcat P180x
Avanti during autonomous flight
<http://www.jetcatamericas.com>, Photo Credit: Aerospace Research Center
Presenter: Ross H. 4

Problem Definition

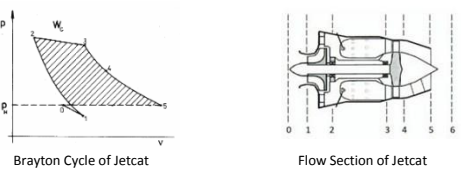
- During flight tests performed last year, data was collected which revealed that engine performance was marginally controllable during dynamic phases of flight
- If engine performance continued to diverge from stable operation, the Avanti could have crashed
- The ability to effectively control the UAV relies on being able to predict the engine's response to different throttle inputs
- **The engine manufacturer does not collect nor provided dynamic performance data**



Presenter: Ross H. 5

Literature Review

- Previous research focused on thermodynamic characterization of the Jetcat
- Can be used to predict thrust data at steady state engine conditions
- Lack of information on dynamic models for transient response



Brayton Cycle of Jetcat
Flow Section of Jetcat
[1] Fozo, Ladislave. IEEE. Pgs 2-3.
Presenter: Hamil S. 6

Project Deliverables

- Goal: Develop a mathematical model that predicts thrust output for a given throttle input

- An accurate engine model will allow Dr. McCrink to more effectively program UAV control
- Making the UAV better, safer, faster, and go further

<https://flyfpv.com>

Presenter: Tommy M.

7

System Modeling Techniques

Analytical Derivation

- Model Physics in Jet Engine
 - Thermodynamics
 - Heat transfer
 - Combustion
 - Compressible flow dynamics
- Find transfer function through

System Identification

- Obtain thrust data through experimental means
- Curve fit the data to determine

Presenter: Tommy M.

8

Experimental Set Up

- Experimental thrust data required at various wind speeds

Current thrust stand used to take Jetcat data

- Mounts in 3ft x 5ft wind tunnel
- Resolves thrust within 1 Newton of force
- (max force is 180N)

- The team needs to make a new thrust stand that meets suitable for transient experiments

<https://rcexplorer.se>

Presenter: Tommy M.

9

Experimental Set Up

Different Thrust Stand Configurations

Linear Thrust Stand in Bolz Hall

Moment Arm Thrust Stand

Presenter: Mark L.

10

Electrical System

- Use a pre-existing Electrical Control Unit (ECU)
- Determine multiple parameters by extracting data from ECU
 - Fuel flow
 - Rotations per minute (RPM)
 - Exhaust gas temperature

[1] <http://www.vspkpeak-modell.de> [2] <https://www.der-schweighofer.net/>

Presenter: Hamil S.

11

Decision Matrix

Design Elements				1 is worst 5 is best	
	Weight	System Identification	Analytical Derivation	Linear Bearing Test Stand	Moment Test Stand
Analytical Complexity	3	3	1	4	4
Accuracy of Model	5	5	4	2	4
Cost	1	2	5	5	3
Ease of Experimentation	4	3	3	4	5
Total		51	40	43	55

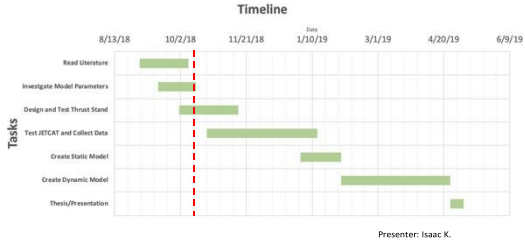
Presenter: Mark L.

12

Project Milestones

Milestones Achieved:

- ✓ Conducted literature review
- ✓ Identified parameters needed to construct model
- ✓ Began design of a thruststand



13

Project Milestones

Upcoming Tasks:



Budget:

Future Cost Considerations	
Item	Projected Cost (\$)
Thrust Stand Material	300
Electrical Equipment	600
Fuel	75
Total:	\$975

Presenter: Isaac K.

14

Questions?

15

Preliminary Design Review

11/6/2018

THE OHIO STATE UNIVERSITY
COLLEGE OF ENGINEERING

Preliminary Design Review Presentation

Team JetCat
Ross Heidersbach, Isaac Khan, Mark Luke, Tommy Malkus, Hamil Shah

Overview

Project Overview
Initial Concept
Updated Thrust Stand Design
System Identification Approach
Concluding Remarks

Project Overview

Goal

- Develop a plant model for the JetCat P180

Method

- Create model via system identification
 - Need a thrust stand and electrical system for data collection

First Design Iteration

- Based structure design off of test stand in Bolz Hall
- Four beam vertical supports with JetCat cradled in center
- Static structure rotating on mostly frictionless hinge point
- Control resolution from stand geometry
- Multiple beams to minimize deflection and stress experienced by stand



Thrust Measurement Considerations

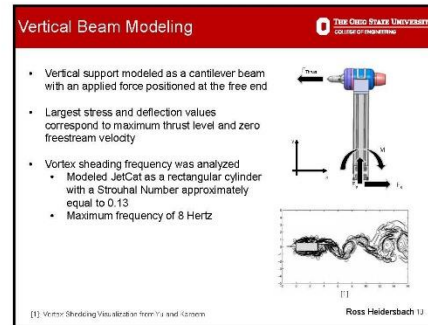
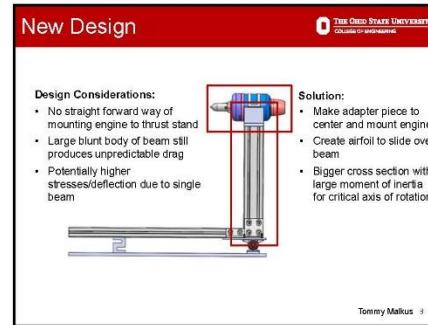


- Max Load Cell Capacity = 50 lbs
- Max Thrust = 44 lbs
- One-to-One force amplification with adjustable load cell location
 - L = 18 inches

Problems with First Design

- Four beam design subject to twist about z and x axis
- Blunt beam geometry could cause strange flow behind thrust stand
- Excess beams and fasteners complicate alignment of engine
- Increased error propagation with additional beams





Beam Size Selection

Standard T-Slotted aluminum extrusions were selected for analyzes

Part Number	Width (mm)	Thickness (mm)	Stress (Mpa)	Safety Factor	Lateral Displacement (mm)	Angular Displacement (Degrees)	Natural Frequency (Hz)
49-4000	90	10	17.46	30.11	0.222	0.142	65.17
49-4001	40	40	1.02	20.4	0.382	0.110	54.3C
49-4004-Lite	40	40	17.46	22.9	0.386	0.115	52.2D
49-4004-Lt	40	40	17.71	17.9	0.106	0.174	53.7F
49-4005	90	20	2.05	20.9	0.382	0.136	113.1E
49-4005-Lite	40	40	17.46	20.9	0.117	0.117	104.4G
49-4005-Lt	90	40	5.15	16.5	0.158	0.254	1.0.79
49-4012	120	40	1.63	14.6	0.126	0.375	163.0H

Criteria: Weight, 600, 400, 4040-Lite, 4040-UL, 4080, 4080-Lite, 4080-UL, 4012

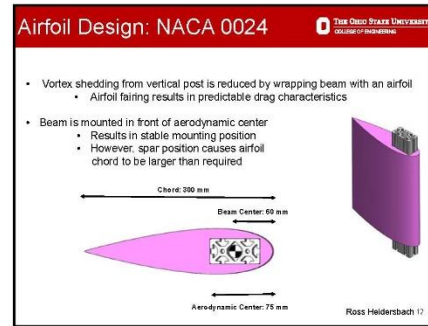
Area: 4, 5, 4, 4, 4, 3, 2, 3, 2

Safety Factor: 2, 5, 3, 2, 2, 4, 4, 3, 5

Displacement: 4, 8, 2, 7, 2, -1, 5, 3, 4

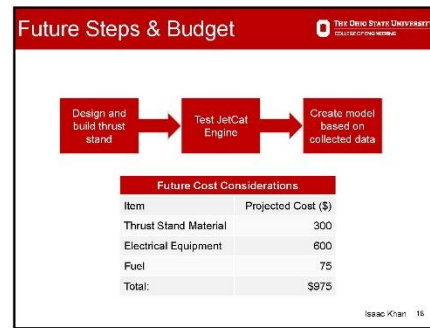
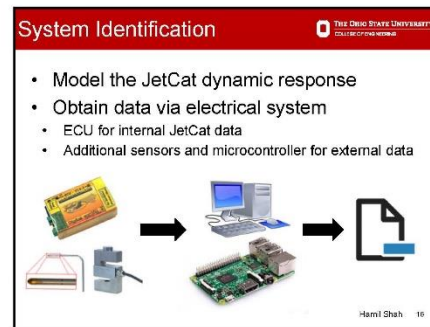
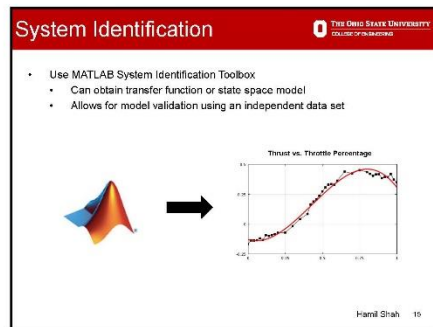
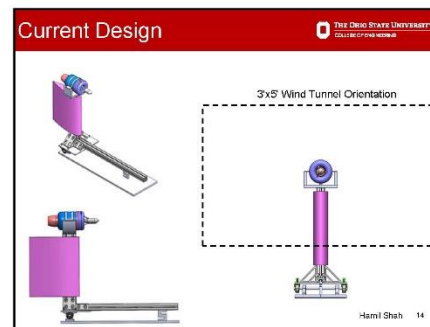
Total: 0, 50, 50, 28, 28, 16, 52, 30, 34

Ross Heidersbach 11



Airfoil Concept Scoring			
Criteria	Weight	NACA 0012	NACA 0024
Coefficient of Drag	4	5	4
Chord Length	5	3	4
Area	3	2	3
Weight	1	3	4
Total	-	44	49

NACA 0024 Airfoil Design Chosen | Ross Heidensbach 13



Areas of Concern

The Ohio State University
COLLEGE OF ENGINEERING

Possible Problems

- Sampling rate and noise of collected data
- Max load cell rating for 50 lbs
- Accuracy of load cell data dependent on full scale range

Hamil Shah 19

Questions?

Appendix

Load Cell Concept Scoring

The Ohio State University
COLLEGE OF ENGINEERING

Criteria	Weight	50 lb	100 lb
Price	2	5	3
Accuracy	5	5	4
Resolution	3	3	3
Safety	4	2	5
Total	-	62	55

100 lb Load Cell Chosen 22

Airfoil Concept Data

The Ohio State University
COLLEGE OF ENGINEERING

Criteria	NACA 0012	NACA 0024
Price	-	-
Coefficient of Drag	-	20% higher
Chord Length	0.45 m	0.30 m
Area	0.21 m ²	0.14 m ²
Weight	152.49 g	131.73 g

NACA 0024 Airfoil Design Chosen 23

Natural Frequency Calculations

The Ohio State University
COLLEGE OF ENGINEERING

- Natural Frequency of a Cantilever Beam
- Frequency of Vortex Shedding

$$\omega_N = 1.875^2 \sqrt{\frac{E * I}{M * L^3}}$$

$$\omega_N = \frac{(St)(U)}{L}$$

- E=Young's Modulus
- I=Area Moment of Inertia
- M=Mass of Beam
- L=Length of Beam
- St=Strouhal Number
- U=Freestream Velocity
- L=Characteristic Length

24

Critical Design Review Presentation

12/7/2018

 THE OHIO STATE UNIVERSITY
COLLEGE OF ENGINEERING

Critical Design Review Presentation

Team JetCat
Ross Heidersbach, Isaac Khan, Mark Luke, Tommy Malkus, Hamil Shah

 THE OHIO STATE UNIVERSITY
COLLEGE OF ENGINEERING

Overview

- Project overview
- Thrust stand concept
- System identification approach
- Project schedule
- Future tasks

Tommy Malkus 2

 THE OHIO STATE UNIVERSITY
COLLEGE OF ENGINEERING

Project Overview

Goal

- Develop a system model for the JetCat P180
 - How does the Jet respond to throttle inputs?
 - How does this change with wind speed?

Method

- Design and build test stand for data collection
- Run experiments and create model via system identification methods

Tommy Malkus 3

 THE OHIO STATE UNIVERSITY
COLLEGE OF ENGINEERING

Process Flowchart

```
graph TD; A[Design & Build Thrust Stand] --> B((Σ)); B --> C[Collect Data]; C --> D[Perform System Identification]; D --> E{Test Model}; E --> F[Model Validated]; F --> G[Update Testing approach]; G --> B;
```

Tommy Malkus 4

 THE OHIO STATE UNIVERSITY
COLLEGE OF ENGINEERING

Final Test Stand Design

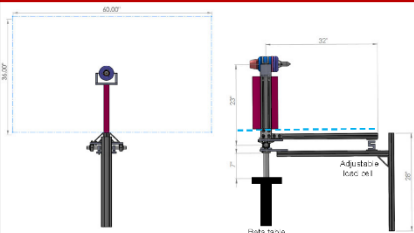
- Moment arm design transmits force to load cell
- Variable load cell location for force de-amplification
- Airfoil type fairing to reduce shedding
- Can be easily installed in the 3"x5" wind tunnel via shaft mount



Tommy Malkus 5

 THE OHIO STATE UNIVERSITY
COLLEGE OF ENGINEERING

Final Design Dimensions



Wind Tunnel View

Side View

Adjustable load cell

Tommy Malkus 6

Vertical Beam Modeling

THE OHIO STATE UNIVERSITY
COLLEGE OF ENGINEERING

- Vertical support modeled as a cantilever beam with an applied force positioned at the free end and weight located at C.G.
- Largest stress and deflection values correspond to maximum thrust level and zero freestream velocity
- Vortex shearing frequency was analyzed
 - JetCat Strouhal Number: 0.13
 - Maximum frequency: 8 Hertz

Vertical Beam Characteristics

Width (mm)	Thickness (mm)	G_{ext} (MPa)	Safety Factor	Lateral Displacement (mm)	Natural Frequency (Hz)
80	40	3.95	72	0.088	110

Ross Heidersbach 7

Horizontal Beam Modeling

THE OHIO STATE UNIVERSITY
COLLEGE OF ENGINEERING

- Horizontal support modeled as a simply supported beam subjected to an applied moment and intrinsic weight
- Hinged location is subjected to the largest internal moment and corresponds to the beam's critical point
- Deflection estimates rely on superposition due to complex loading

Horizontal Beam Characteristics

Width (mm)	Thickness (mm)	G_{ext} (MPa)	Safety Factor	Lateral Displacement (mm)
40	40	28.78	12	0.13

Ross Heidersbach 8

Bolting Group Calculations

THE OHIO STATE UNIVERSITY
COLLEGE OF ENGINEERING

- Four bolt groups were selected for failure mode analysis
- Groups 1 and 3 primarily subject to shear stress
- Groups 2 and 4 primarily subject to axial stress

Bolting Group 1 Tension using Max Shear Stress Failure Theory

Bolting Group 1 Safety Factor using Max Shear Stress Failure Theory

Mark Luke 9

Test Stand Failure Modes

THE OHIO STATE UNIVERSITY
COLLEGE OF ENGINEERING

- Max thrust limited by load cell
- Larger jet engines could be tested but would require larger load cell

Failure Modes

COMPONENT	MATERIAL ALLOWABLE JET THRUST (LBS)
HORIZONTAL BEAM	490
VERTICAL BEAM	2880
BOLT GROUP 1	311
BOLT GROUP 2	525
BOLT GROUP 3	360
BOLT GROUP 4	640
LOAD CELL	70

Mark Luke 10

Prototype Plan

THE OHIO STATE UNIVERSITY
COLLEGE OF ENGINEERING

- Assembly Jet Stand
 - Fabricate parts from CDME or Scott Lab
 - Most parts off the shelf and easy to assemble
- Test JetCat outside wind tunnel
 - Trouble shoot sensors and electrical equipment
 - Calibrate load cell
 - Test MATLAB System Identification Toolbox
- Wind tunnel data collection for system modeling

Hamil Shah 11

Data Collection

THE OHIO STATE UNIVERSITY
COLLEGE OF ENGINEERING

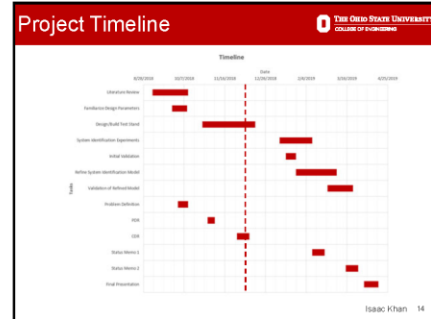
- Set up stand in wind tunnel
- Set airspeed and vary throttle input
- Collected data for each trial
 - Thrust (from load cell)
 - RPM
 - EGT
 - Fuel flow
- Need to determine data needs
 - Wind speed interval (i.e., 1, 5, or 10) from 20-100mph
 - # of trials required

Hamil Shah 12

System Identification Model

- Utilize collected data to create a model
- Multiple modeling options
 - Linear
 - Recursive Least Squares
 - Non-Linear
 - Nonlinear ARMAX
 - Unscented Kalman Filter
 - Machine Learning
- Model different throttle ranges

Hamil Shah 13



Milestones Achieved

- Designed thrust stand that went through vetting process with experts
- Iterated design with feedback given
- Investigated non-linear modelling methods
 - Matlab System Identification Toolbox

Isaac Khan 15

Future Steps & Budget

Cost Considerations	
Item	Projected Cost (\$)
Thrust Stand Material	575
Electrical Equipment	600
Fuel	75
Total:	\$1,250

Isaac Khan 16

Areas of Concern

Areas of concern include:

- Sampling rate or sampling time mismatch
 - Data should start at the same time
- Choice of computer software packages (LabView, Matlab)
 - What computer will be used
- Ill selection of parameters for plant model
 - Using uncorrelated data
- Weather on day of experiments
 - Wind speed and direction, changing atmospheric conditions
- Hysteresis on thrust throttle correlation

Isaac Khan 17

Questions?

Final Design Review Presentation

Project Schedule

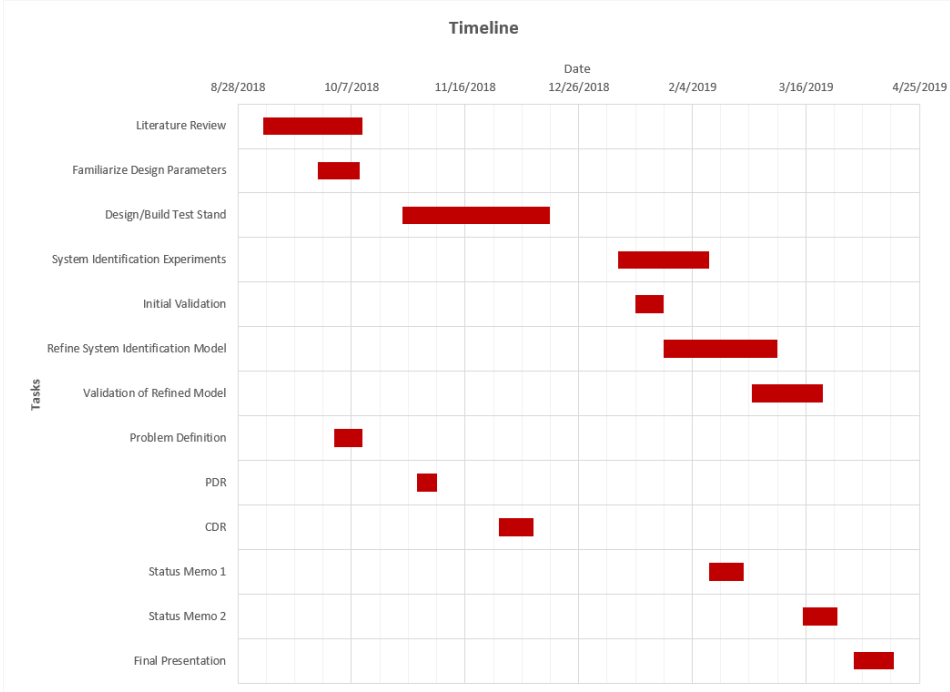


Figure A.1: Gantt Chart

Team Meeting Notes

Meeting Notes

Meeting with Dr. Matt McCrink

September 6th, 2018

Aerospace Research Center

Initial Meeting with Industry Sponsor

1. Representative Models
 - a. P-180 – Model we will be working with
 - i. Open Loop Plant Model **needed**
 - b. P-90 – Another model offered by JetCat, same physical dimensions, less output thrust
 - i. We will **not** be working with this turbojet
2. Validation method must be created
 - a. Why does said validation model work?
 - b. How have others validated results?

Tasks for next meeting

1. Literature Review
 - a. Find google scholar articles of research groups that have worked with turbojet engines
 - b. Refine search further and further to find papers that
2. Contact Dreamworks RC, JetCat USA for warranty info

Meeting Notes

Meeting with Dr. Matt McCrink

September 20th, 2018

Aerospace Research Center

Last time à This week

1. Discussed scholarly papers found and their impact to the current problem set up
 - a. Brought ~7 articles that everyone read and discussed with Dr. McCrink potential problem definitions to answer
 - i. Steady State – Articles had information about this type of modeling for P180
 - ii. Transient – Not many articles had info on this type of modeling for P180
2. Contacted Dreamworks RC, JetCat USA
 - a. Company was evacuating due to hurricane threat.

This week

1. Canonical Modeling
 - a. Performance derogation as wind velocity increases
 - b. Dynamic modeling is more experimentally established
 - i. We are not interested in startup of the P180 JetCat
 1. We are interested in snap response due to thrust command given
2. Energy Storage Systems as means of determining order of plant model
 - a. Inertial effects
 - b. Combustion of fuel
 - c. Damping effects?
3. System Identification
 - a. “when you poke it can you determine a model for it...have an input/output and focus in on what happens in the middle”
4. MathWorks Depository
 - a. Shift through code from scholarly papers for useful snippets
 - i. See how they got their diagrams
5. Test Stand
 - a. Current test stand can be used, but a more elegant stand can be developed
6. Interface for JetCat
 - a. ECU measures multiple parameters
 - i. Doesn’t report this information, often used for internal calculations
 - ii. Unable to measure engine pressure ratio, but through physical modeling, it can be calculated based on E.G.T.

Parts and Assembly

Take Away

1. Output Error --> Canonical Form
 - a. Use of System Identification tool in Matlab
2. Static Performance Model - Thermodynamic characterization
3. Dynamic Model – moving dynamics of JetCat engine

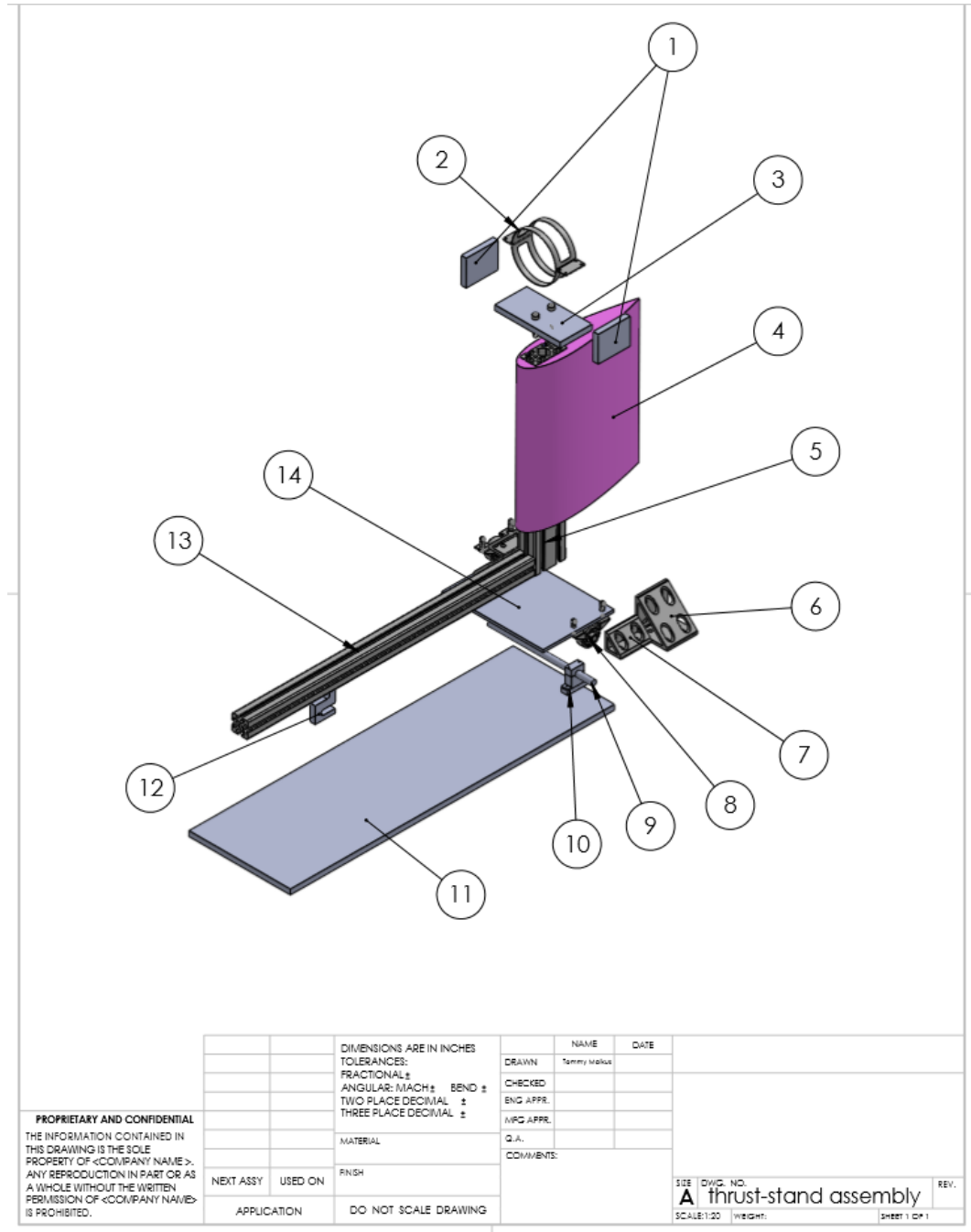


Figure A.2 Exploded View of Preliminary Design

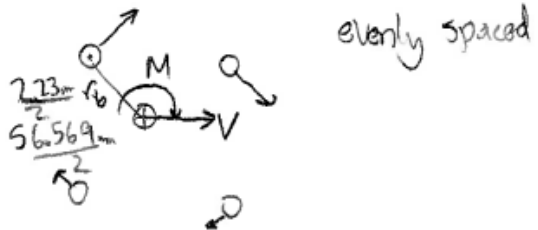
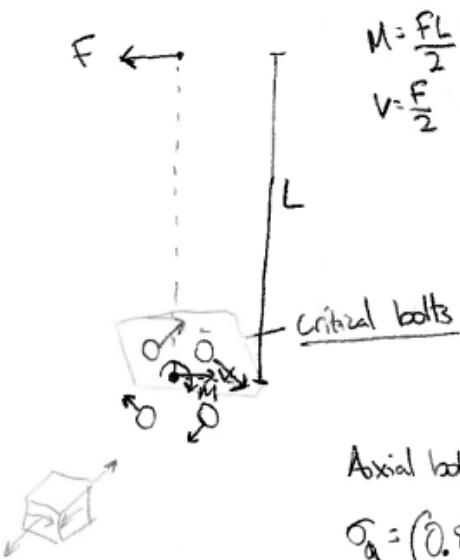
Bolts			
Size	Part #	Qty	Cost \$
Adapter Materials			
M5x0.8 30mm Lg Flat head	92125A220	25	\$6.55
M8x1.25 x 40mm Lg Flat head	92125A294	10	\$6.22
Beams and Brackets			
Tslot nut/bolt M8x16mm lg	5537T455	4/pack x 6packs =24	\$18.54
M8x1.25 x 30mm lng	91239A428	25	\$8.49
M8x1.25 nuts	90591A161	100	\$5.44
Shaft and Mount			
3/8x24 x 1-1/4" lg Button head	92949A653	5	\$5.54
3/8x24 locknut	96278A531	10	\$6.25
1/4-20 Hex nut locknut	90675A029	100	\$5.42
1/4-20, 1-1/4" long socket head	91251A544	50	\$11.80
			Total: \$74.25

Electrical Materials		
Component	Source	Cost \$
ECU	JETCAT USA	-
Microcontroller (Arduino)	Adafruit	\$20.00
Misc. Cables and Materials	Adafruit	\$30.00
New Load Cell		\$500.00
Pressure Sensor**	Omega	-
** = Provided By Dr. McCrink		Total: \$550

Figure A.3 Breakdown of the Additional Materials from the Detail Design B.O.M.

Bolt Stress Analysis

Bolting Calcs group 1



Preload $\approx 85\%$ proof strength

~~1.25M8~~ proof strength = $225 \text{ MPa} \rightarrow p_5 499, T13.5$
low grade steel

$A_b = 37.6 \text{ mm}^2 \rightarrow p_5 491, T13.2$
course thread

Axial bolt load = preload stress

$$\sigma_a = (0.85)(225 \text{ MPa}) = 191.25 \text{ MPa}$$

Shear Stress

$$\tau_b = \sqrt{\left(\frac{M r_b}{\frac{1}{4} A_b r_b^2}\right)^2 + \left(\frac{V}{\frac{1}{4} A_b}\right)^2}$$

Shear induced from moment

Shear from reaction

VM stresses (1 plane)

$$\sigma_{1,2} = \frac{\sigma_b}{2} \pm \sqrt{\left(\frac{\sigma_b}{2}\right)^2 + \tau_b^2}$$

$$\sigma_3 = 0$$

$$\sigma_{eq} = \sqrt{\frac{1}{2} (\sigma_1 - \sigma_2)^2 + \sigma_1^2 + \sigma_2^2}$$

Force required for preload

$$F_i = \sigma_a \cdot A_b = 7191 \text{ N}$$

$$T_i = \left[\frac{1}{2} \left(\frac{L \cos \theta + \pi d_b \mu}{\pi d_b \cos \theta - L \mu} \right) + (25 \mu) F_i d_b \right]$$

$$= 13600 \text{ Nmm} \approx 13.6 \text{ Nm}$$

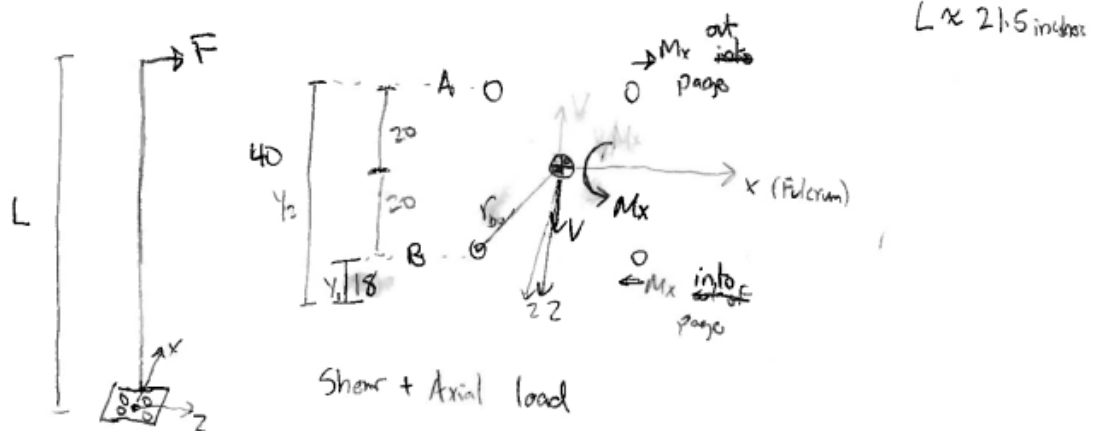
$$\theta = 30^\circ$$

$$L = 1.25$$

$$d_b = 8 \text{ mm}$$

$$\sigma_{yp} = 240 \text{ MPa}$$

Bolt Group 2



Determine axial load on bolts $\sqrt{\frac{F \cdot L}{2}}$ $y = 20, -20 \text{ mm}$

$$F_A = F_m + F_i \rightarrow F_m = \left(\frac{k_b}{k_b + k_m} \right) A_b \left(\frac{(M_x) Y}{\sum A_b Y^2} \right) \rightarrow A_b (20^2 + (-20)^2)$$

$$k_m = \frac{1}{k_{m1} + k_{m2}}$$

k_{m1} = T-slot corner bracket = aluminum
 k_{m2} = T-slot = aluminum ~~with same rate~~

$$k_{m1} = \frac{\pi (d_{m1}^2 - d_{ub}^2) E_{m1}}{4 L_{m1}}$$

$d_{m1} = 2 \text{ cm}_b \leftarrow \text{nominal bolt diam} = 8 \text{ mm}$
constant diameter cylinder approximation in force-flow regime

$$L_{m1} = 6 \text{ mm}$$

$$E_{m1} = 68.9 \text{ GPa}$$

$$k_{m2} = \frac{\pi (d_{m2}^2 - d_{ub}^2) E_{m2}}{4 \cdot L_{m2}}$$

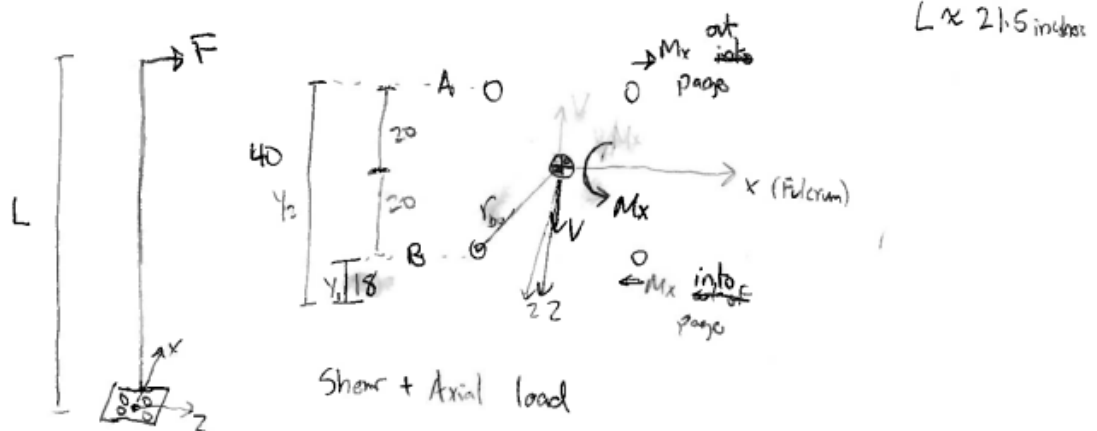
Same but $L_{m2} = 4.5 \text{ mm}$

$$k_b = \frac{\pi d_b^2 E_b}{4 L_{eff}}$$

$$L_{eff} = L_{m1} + L_{m2} \quad d_b = 8 \text{ mm}$$

$$E_b = 200 \text{ MPa (steel)}$$

Bolt Group 2



Determine axial load on bolts $\sqrt{\frac{F \cdot L}{2}}$ $y = 20, -20 \text{ mm}$

$$F_A = F_m + F_i \rightarrow F_m = \left(\frac{k_b}{k_b + k_m} \right) A_b \left(\frac{(M_x) Y}{\sum A_b Y^2} \right) \rightarrow A_b (20^2 + (-20)^2)$$

$$k_m = \frac{1}{k_{m1} + k_{m2}}$$

k_{m1} : T-slot corner bracket: aluminum
 k_{m2} : T-slot: aluminum ~~with same rate~~

$$k_{m1} = \frac{\pi (d_{m1}^2 - d_{ub}^2) E_{m1}}{4 L_{m1}}$$

$$d_{m1} = 2 \text{ cm} \leftarrow \text{nominal bolt diam} = 8 \text{ mm}$$

\uparrow constant diameter cylinder approximation in force-flow regime

$$L_{m1} = 6 \text{ mm}$$

$$E_{m1} = 68.9 \text{ GPa}$$

$$k_{m2} = \frac{\pi (d_{m2}^2 - d_{ub}^2) E_{m2}}{4 \cdot L_{m2}}$$

$$\text{Same but } L_{m2} = 4.5 \text{ mm}$$

$$k_b = \frac{\pi d_b^2 E_b}{4 L_{eff}}$$

$$L_{eff} = L_{m1} + L_{m2} \quad d_b = 8 \text{ mm}$$

$$E_b = 200 \text{ MPa (steel)}$$

Min preload to keep bolts from joint separation

$$F_{mA} = F_b - F_i$$
$$(F_b = \left(1 - \frac{k_b}{k_b + k_m}\right) A_{b0} \left(\frac{(M_x)y}{\sum A_{b0}y^2}\right))$$

F_{mA} must remain negative to determine minimum preload!

$$F_b = 312 \text{ N}$$

Choose preload of 1000 N $\mu = 0.15$

$$F_i = 1000 \text{ N} \rightarrow T_i = \left[\frac{1}{2} \left(\frac{L \cos \theta + \pi d_b M}{\pi d_b \cos \theta - L \mu} \right) + 625 \mu \right] F_i d_b$$

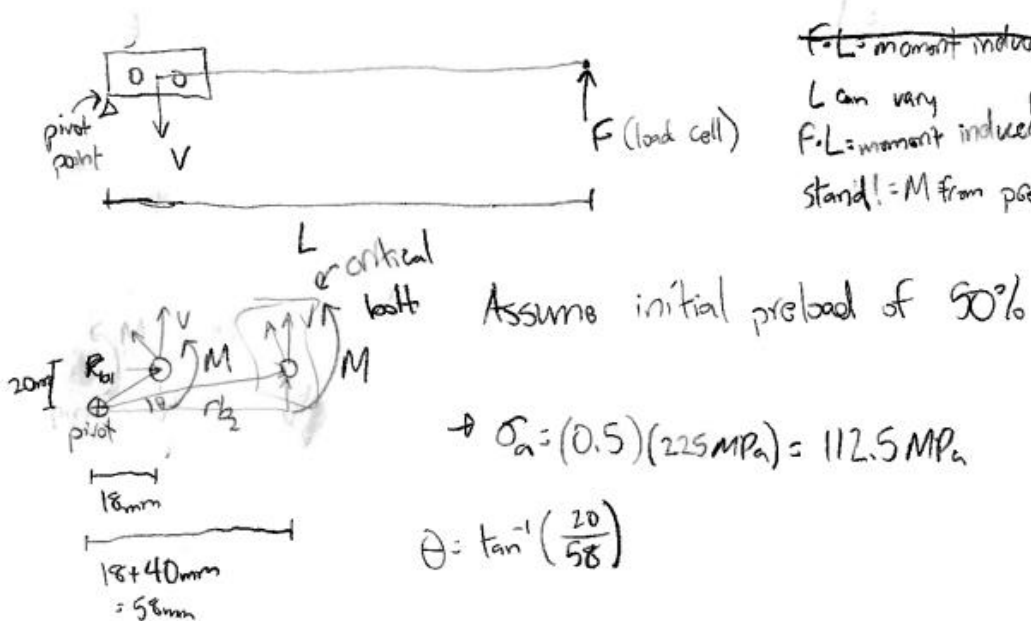
$$T_i = 5.05 \text{ Nm}$$

$$\rightarrow \text{Axial Load: } F_{max} = F_i + F_{on}$$

Rest in MatLab to calculate

Stresses

Bolt group on horizontal beam



F dependent on L distance!

$F \cdot L$ moment induced by thrust!

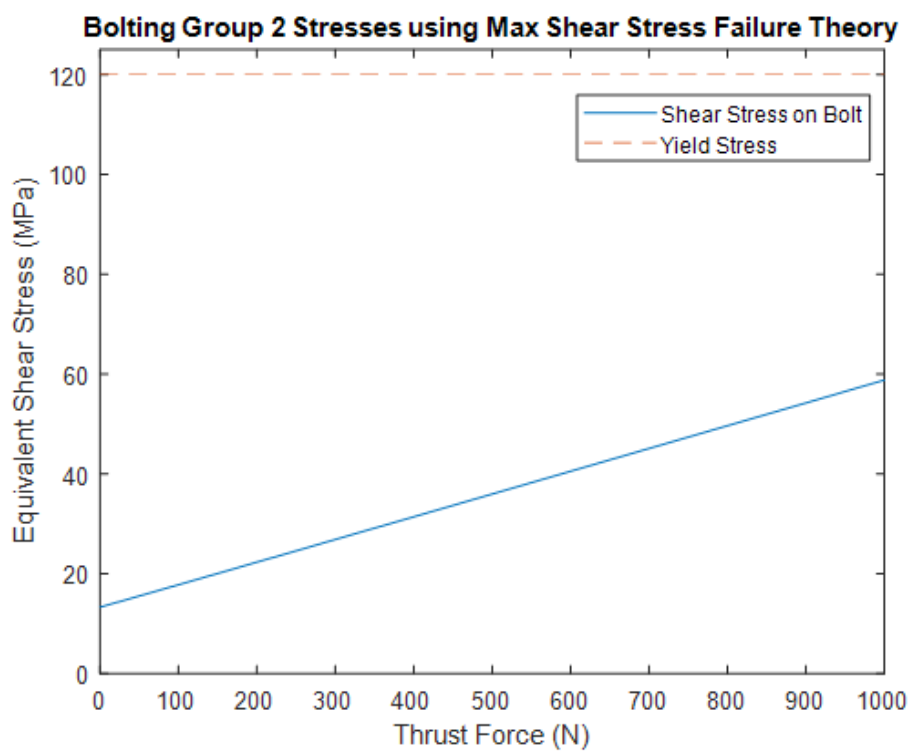
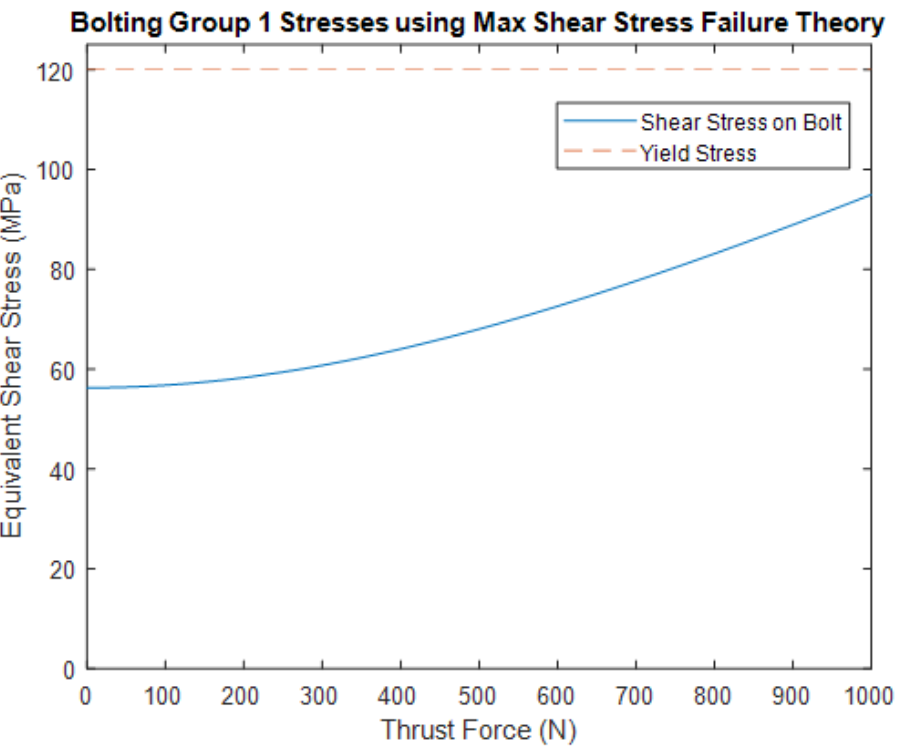
L can vary

$F \cdot L$ moment induced by
standoff $= M$ from previous bolt group!

Shear induced stress

$$\tau_b = \sqrt{\left(\frac{M_b r_o}{2A_b r_b} \sin\theta\right)^2 + \left(\frac{V}{2A_b} + \frac{M_b r_o}{2A_b r_b} \cos\theta\right)^2}$$

Figure A.4: Bolting group calculations for the four different groups.



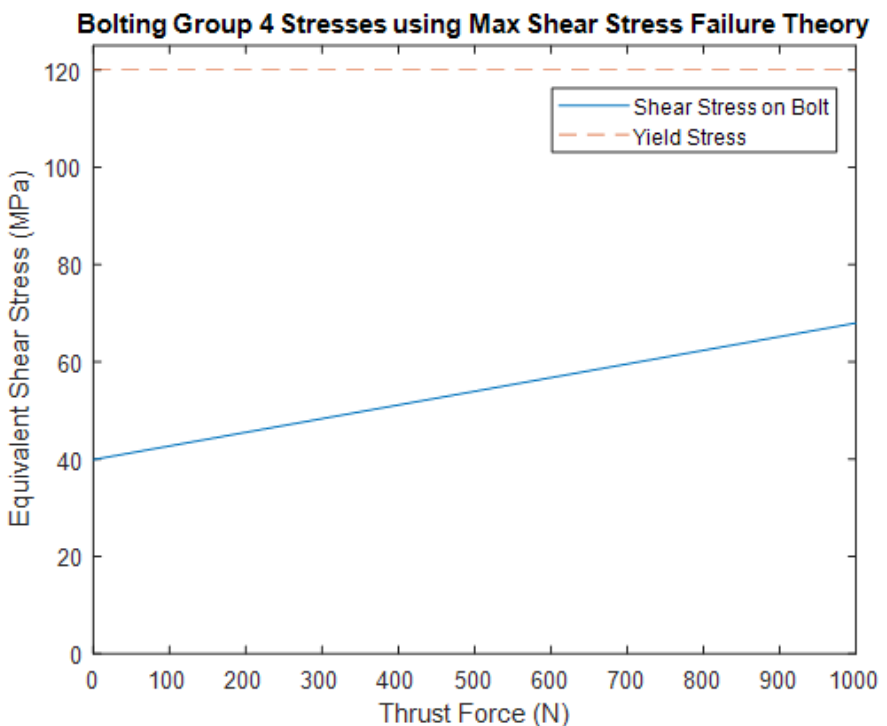
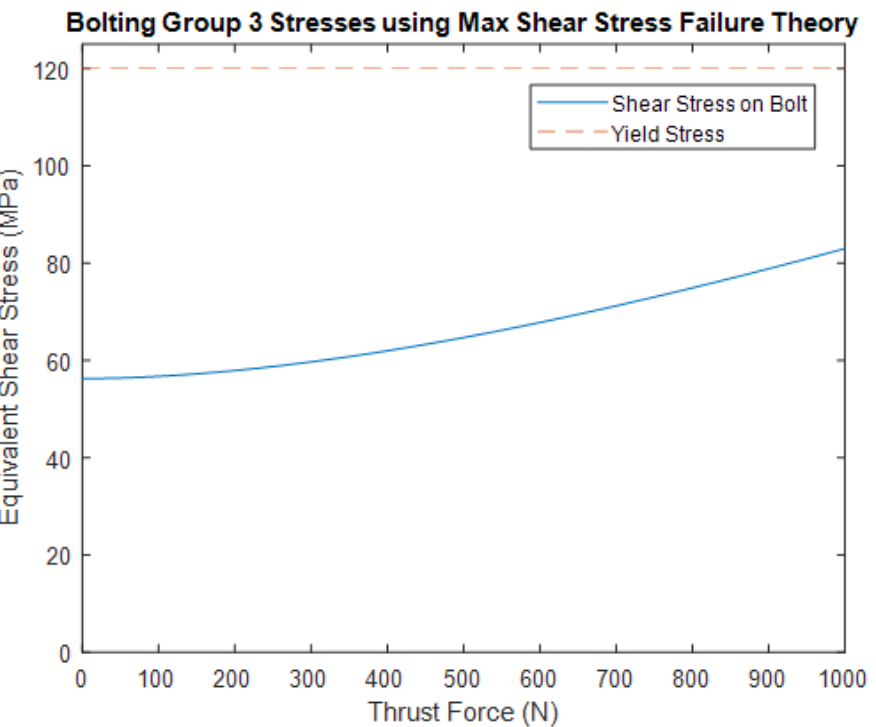
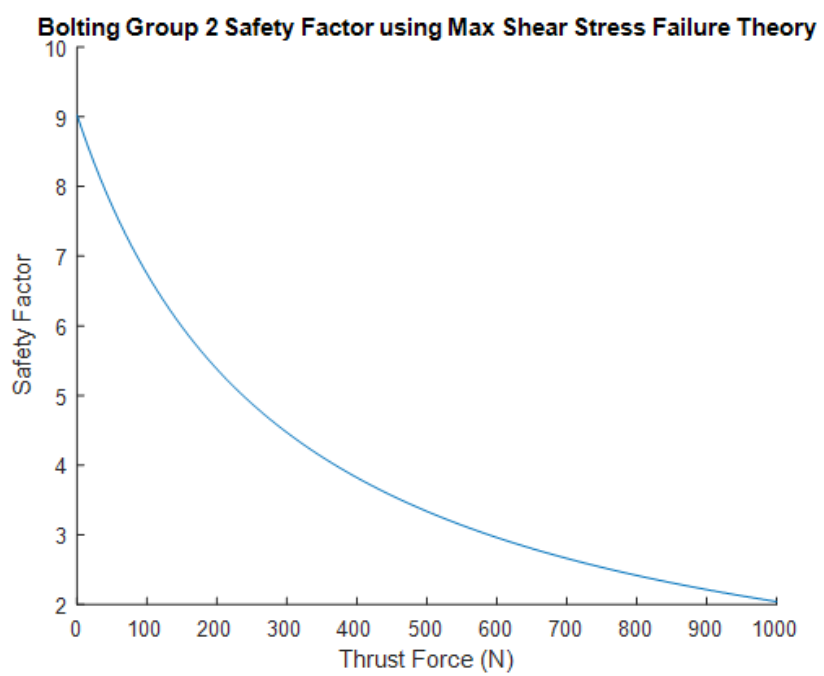
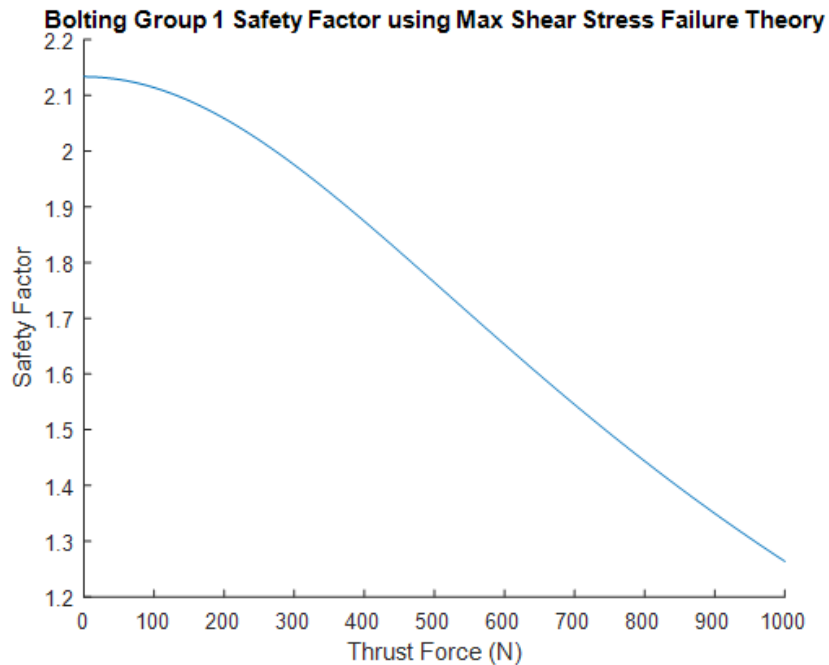


Figure A.5: Bolting group stress figures using max shear stress failure theory.



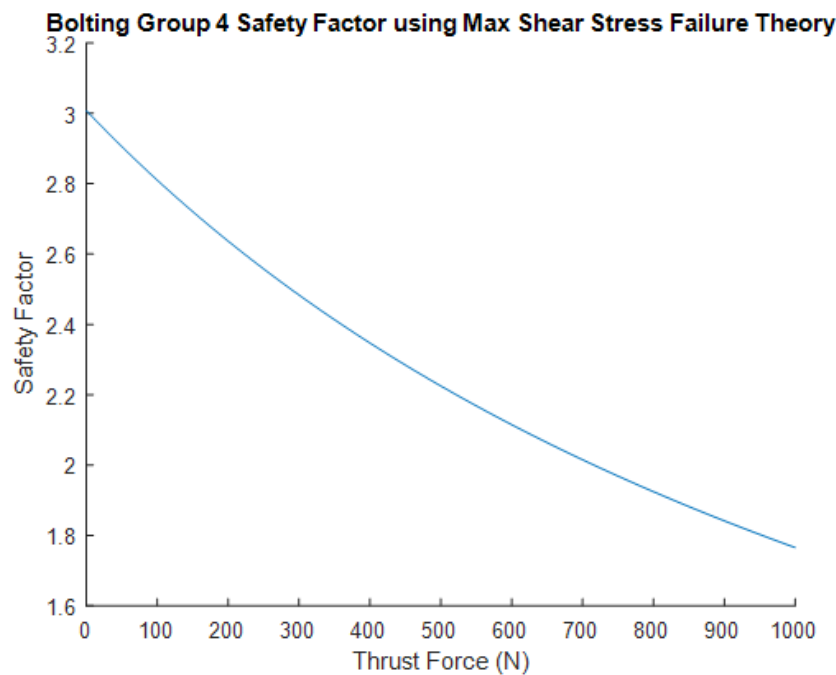
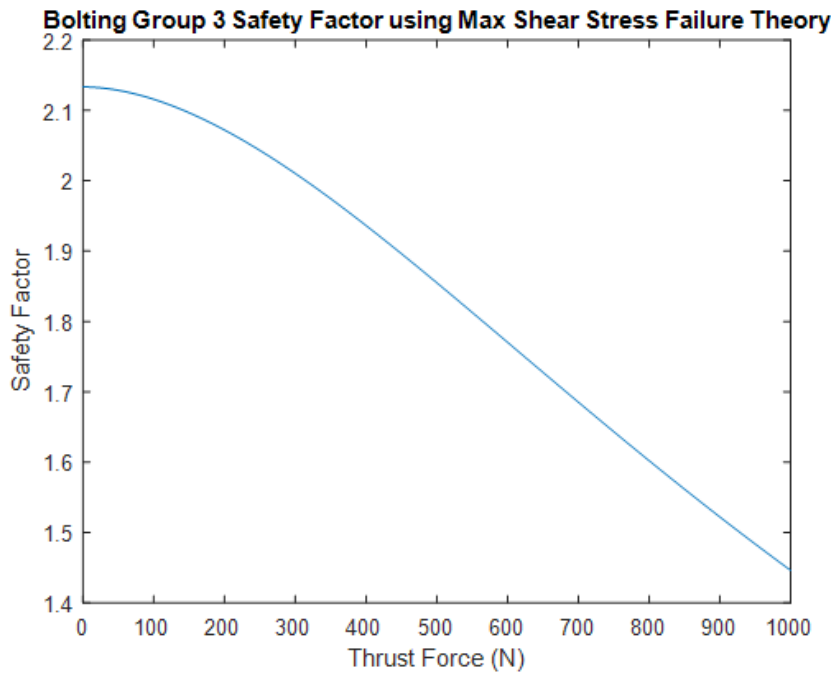


Figure A.6: Bolting group safety factors using max shear stress failure theory.

Load Cell Calibration



Figure A.7: Pulley system used for load cell calibration.

Custom Piece Drawings

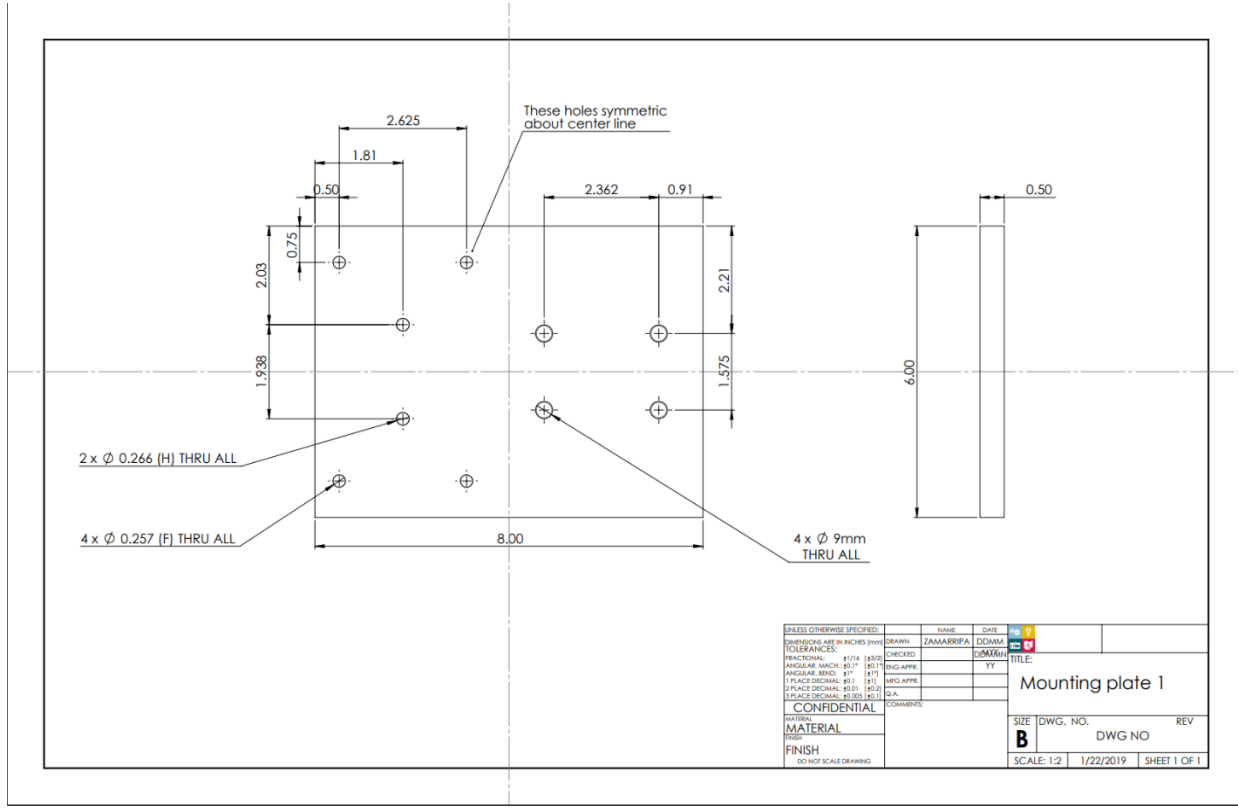


Figure A.8: Base plate one of the jet stand.

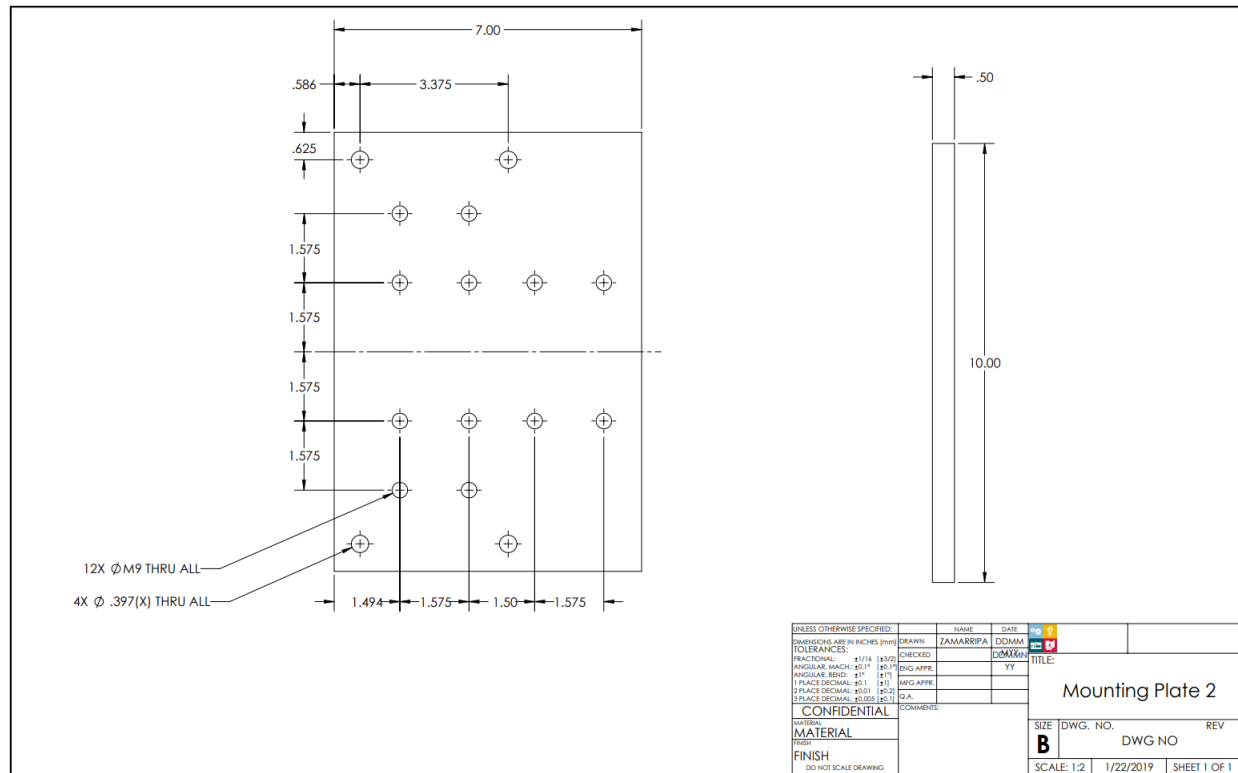


Figure A.9: Base plate two of the jet stand.

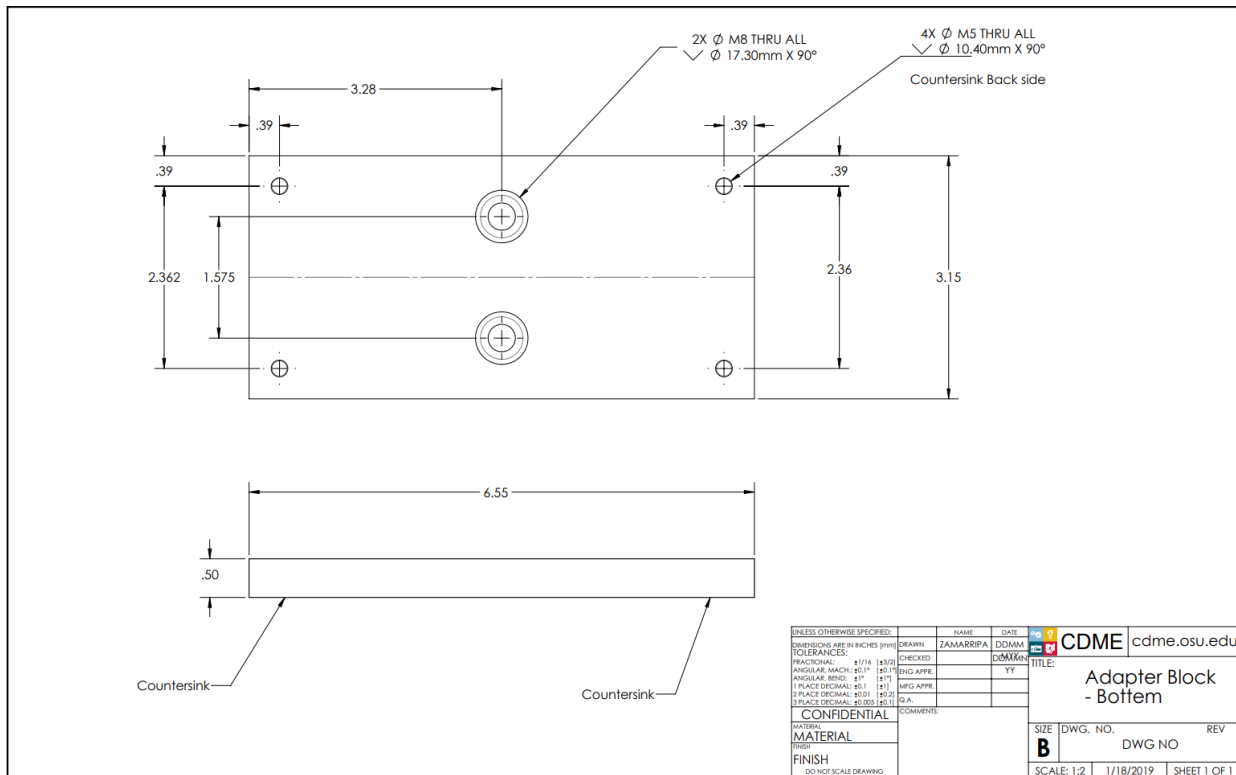


Figure A.10: Bottom block of the engine adapter system.

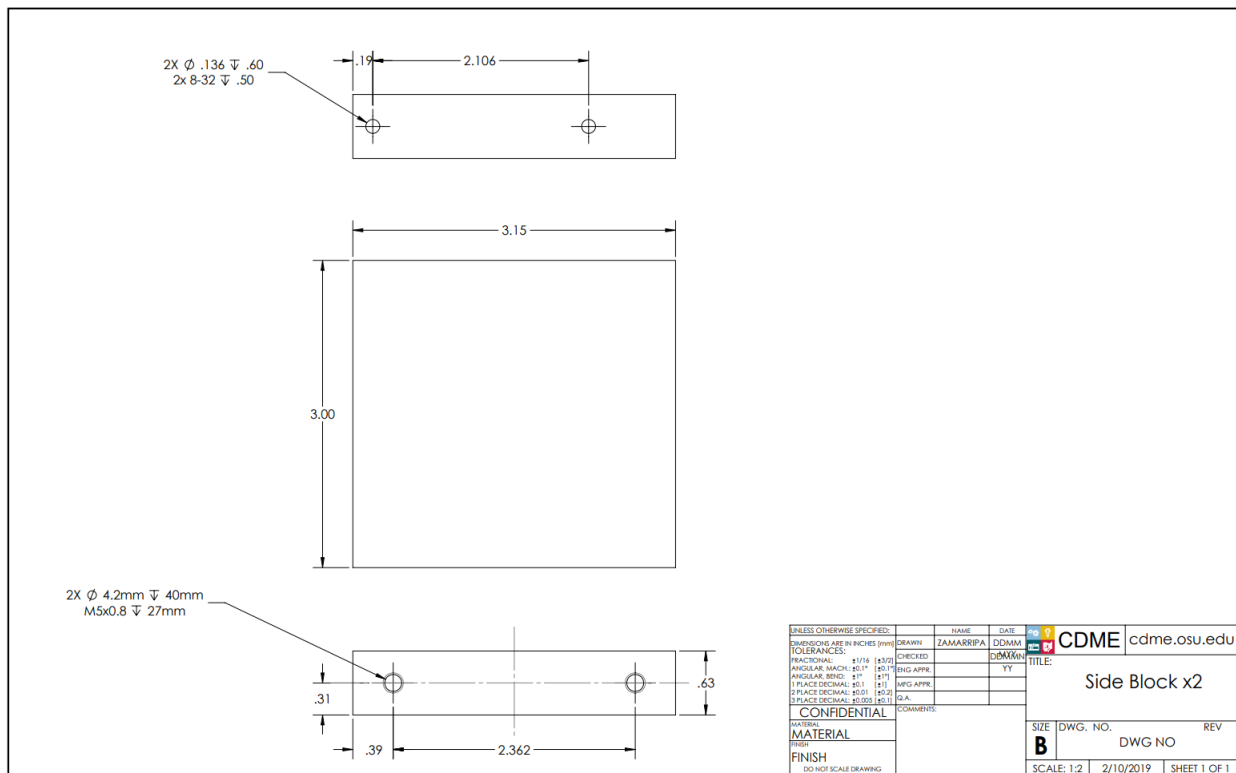


Figure A.11: Side block of the engine adapter system.

